G. Di Martino, A. Iodice, A. Natale and D. Riccio, “Polarimetric Two-Scale Two-Component Model for the Retrieval of Soil Moisture under Moderate Vegetation via L-Band SAR Data”, *IEEE Trans. Geosci. Remote Sens.*, vol. 54, no. 4, pp. 2470-2491, April 2016. DOI: 10.1109/TGRS.2015.2502425.

Polarimetric Two-Scale Two-Component Model for the Retrieval of Soil Moisture Under Moderate Vegetation via L-Band SAR Data

Gerardo Di Martino, *Member, IEEE*, Antonio Iodice, *Senior Member, IEEE*, Antonio Natale, *Member, IEEE*, and Daniele Riccio, *Fellow, IEEE*

***Abstract*—Recently, we have proposed a retrieval technique based on an original polarimetric two-scale model (PTSM), which is able to estimate the volumetric water content of bare soils from polarimetric synthetic aperture radar (SAR) data. In this paper, to extend the field of application of our retrieval technique to moderately vegetated soils, we combine the PTSM with a randomly oriented dipole-cloud volumetric scattering model, thus obtaining a polarimetric two-scale two-component model (PTSTCM). By using this model we show that, in principle, suitable combinations of the polarimetric SAR channels, i.e., "modified copolarized ratio" and "modified copolarized correlation coefficient," are related only to the surface parameters because the dependence on the unknown volumetric contribution intensity cancels out. This allows us to retrieve soil moisture from L-band SAR data not only for bare soils but also in moderately vegetated areas, interested by a nonnegligible volumetric scattering contribution, provided that the double-bounce scattering component is negligible. In addition, describing the surface component by using the PTSM allows us to mitigate the well-known problem of overestimating the volume component, which affects most model-based target decompositions and that may lead to the so-called "negative power problem." Both the performance and validity limits of the estimation method are assessed by comparing the obtained soil-moisture retrieval results to "*in situ*" measurements. To this aim, data from SMEX'03 and AGRISAR'06 campaigns available in literature are considered. They refer to sites with a flat topography. In particular, we employ the AGRISAR database, which includes data from several fields covering a period that spans all the phases of vegetation growth, to explore the validity range of the method in terms of vegetation height. Results of PTSTCM are also compared with those of available three-component methods (3CMs) employing more simplified surface scattering models. It has turned out that the use of the PTSTCM provides more accurate results for low vegetation (average modulus of soil moisture relative error for vegetation height smaller than 50 cm: 18.5% for the PTSTCM and 34% for the 3CM). Conversely, for higher vegetation, 3CMs should be more conveniently employed (average modulus of relative error for vegetation height greater than 50 cm: 17.5% for the 3CM and about 100% for the PTSTCM). A simple method to adaptively and automatically (i.e., based on measured data) select between PTSTCM and 3CM on a pixel-by-pixel basis is finally suggested, leading to a less than 20% average modulus of relative error on the retrieved soil moisture for the considered fields over the entire vegetation growth cycle.**

***Index Terms*—Polarimetry, rough surfaces, soil moisture retrieval, synthetic aperture radar (SAR).**

I. Introduction

IN MANY agricultural, hydrological, and meteorological applications, knowledge of soil moisture content is of fundamental importance: For instance, it is an essential piece of information for the prediction of crisis events such as floods and landslides, as well as for precision farming [1]. Therefore, in the last decades, ground water content retrieval from multiangle, multifrequency, or multipolarization SAR data has been the subject of extensive research [1]–[23]. Both radiative transfer [2]–[5] and wave approaches [5]–[23] have been proposed, and we here focus on the latter, which can more easily model coherent SAR polarimetric data, with a smaller number of parameters to retrieve. Initially, research in this field mainly addressed bare soils [6]–[10], [12]–[17], [19]. Within this framework, some of the authors of this paper proposed a retrieval technique based on an original PTSM [13], [14], [16], [19], which is able to estimate the volumetric water content of bare soils from polarimetric SAR data in flat areas [13] or in areas with a significant topography [14], [19]. An important feature of the PTSM is that it is able to account for cross-polarization and depolarization effects actually present in measured SAR data even when surface scattering is the only present mechanism. This is achieved by properly considering both the random variation of the local incidence angle and the random rotation of the local incidence plane around the line of sight, which is caused by the terrain large-scale roughness [13], [16]. This is at variance with the X-Bragg model [10], which also accounts for cross-polarization and depolarization, but it only considers a random uniformly distributed rotation of the local incidence plane around the line of sight. The PTSM-based retrieval technique is able to estimate the volumetric soil moisture and the rms of the large-scale roughness slope by using the copolarized and cross-polarized ratios [13] or the copolarized ratio and the copolarized, i.e., HH-VV, correlation coefficient [19]. In fact, these quantities turn out to be independent of soil small-scale roughness. In [13], it was shown that the PTSM retrieval results over bare

Manuscript received March 22, 2015; revised August 3, 2015, September 17, 2015, and October 19, 2015; accepted November 17, 2015.

G. Di Martino, A. Iodice, and D. Riccio are with the Department of Electrical Engineering and Information Technology, University of Naples Federico II, 80125 Naples, Italy (e-mail: gerardo.dimartino@unina.it; iodice@unina.it; daniele.riccio@unina.it).

A. Natale is with the Institute for Electromagnetic Sensing of the Environment, Italian National Research Council, 80127 Napoli, Italy (e-mail: natale.a@irea.cnr.it).

Color versions of one or more of the figures in this paper are available online at http://ieeexplore.ieee.org.

Digital Object Identifier 10.1109/TGRS.2015.2502425

soils are more accurate than those obtained by other similar available techniques, based on Bragg or X-Bragg models.

The performance of techniques aimed at retrieving the moisture content of bare soils, including PTSM, rapidly worsen when an even moderate vegetation is present, so that nonnegligible volumetric and/or multiple-bounce scattering components are present. In order to extend the field of application to vegetated soils, more recently, some techniques for soil moisture retrieval under vegetation cover have been developed [11], [18], [20]–[23]. They are based on polarimetric target decomposition techniques [24]–[36]. Two classes of target decomposition techniques can be identified: The so-called eigenvalue decompositions [24], which separate different scattering contributions by computing eigenvalues and eigenvectors of the coherency matrix (very recently, a related approach [25] based on independent component analysis has been also proposed), and model-based decompositions [26], [27], [29], [30], [32]–[36], which use scattering models for the surface contribution and for the other scattering contributions present in the scene. Hybrid eigenvalue/model-based techniques have been also developed [28], [31]. Since bare-soil moisture retrieval techniques are based on surface scattering models, their extension to include vegetated soils requires the use of model-based decompositions: In fact, available techniques for soil moisture retrieval under vegetation employ model-based [11], [18], [20] or at least hybrid [21]–[23] decompositions. The first and most widespread model-based decomposition is the three-component Freeman and Durden (FD) one [26], which employs the Bragg model for surface scattering, a dihedral Fresnel scattering model for double bounce, and a simple dipole-cloud model for volume scattering from canopy. The FD decomposition has the advantages of simplicity and direct physical interpretability. However, it was recognized [28] that the FD decomposition suffers from the "negative power problem:" In many cases, after removing the retrieved volumetric contribution, the obtained polarimetric covariance or coherence matrix is not positive semi-definite, i.e., it has at least one negative eigenvalue. Of course, this is a nonphysical situation, and it is a clear indication that the employed scattering models are often not adequate to describe the real data. In particular, this problem is mainly caused by the fact that FD decomposition attributes the whole cross-polarization effect to volumetric scattering, thus overestimating this latter component [28]. In fact, apart from volumetric scattering, other possible causes of cross polarization exist: They are listed in the following, together with ways to account for them.

1) Oblique dihedrals that are often present in urban areas: They can be included by adding a fourth scattering component [27], [30] and/or matrix rotation [15], [30], or using a more refined building model [37]; however, this is not necessary if an agricultural area is considered as it is usually the case for soil moisture retrieval.
2) Significant topography that causes an azimuth terrain slope: This can be accounted for by performing a rotation of the scattering matrix [38], [39] or, if topography is known, by including a nonzero mean terrain slope in the surface scattering model [14], [19].
3) Significant soil surface roughness, which causes cross polarization also in the surface scattering component: This can be accounted for by using X-Bragg or PTSM for the surface component.

In addition, another cause for the "negative power problem" recognized in literature is the excessive simplicity of the volumetric scattering model: Enhanced dipole-cloud models [11], [20], [27], [40], [41], or more complex adaptive parametric models [21]–[23], [29], [34] have been therefore proposed.

Based on the given considerations, it is obvious that improvements of models for all scattering components would be required. However, unfortunately, any significant improvement in modeling a scattering component implies that the number of parameters to retrieve increases, which in turn causes the retrieval problem to become ill-posed. Therefore, the models of other components must be further simplified to keep the number of unknown parameters unchanged or, equivalently, some parameters must be arbitrarily *a priori* fixed, or further conditions must be imposed. For instance, techniques employing parametric variable/adaptable vegetation volume models [21]–[23], [29], [34] all use methods to reduce the number of unknown parameters in the surface and double-bounce components by adding constraints. An elegant way to deal with this problem is to use the eigenvalue decomposition for these components and impose their orthogonality, thus employing a hybrid decomposition (model-based for volume scattering and eigen-based for surface and double-bounce components), as in [21]–[23]. However, although it is certainly true that this greatly improves soil moisture retrieval in significantly vegetated areas, it is questionable that this also improves retrieval in moderately vegetated areas: In fact, for the surface component, inaccurate scattering descriptions, not including cross polarization, are still used. In addition, at variance with the case of perfectly conducting scatterers, in the more realistic case of dielectric scatterers, there is no physical reason that imposes orthogonality of surface and double-bounce components.

A heuristic way to avoid the negative power problem without the necessity of improving the scattering models (and hence without increasing the number of unknowns) was proposed in [28] and employed in [20] for soil moisture estimation: It consists in constraining the volume component power to be not larger than the maximum value that allows us to obtain a positive semi-definite remaining coherency matrix (an analytical expression for this value was computed in [28] for the reflection symmetry case, which is of interest for soil moisture retrieval applications). However, although this ensures avoiding the negative power problem, it does not imply that the soil moisture retrieval is improved for moderately vegetated soils: Again, for the surface component, inaccurate scattering models, not including cross polarization, are still used. It must be also noted that obtaining a positive semi-definite remaining coherency matrix does not ensure that the volumetric component is not overestimated, but only that it is not so overestimated as to cause the negative power problem.

Based on the considerations above, we believe that the only way to improve retrieval results in moderately vegetated areas is to improve the surface scattering model by using X-Bragg

or PTSM (and hence introducing an additional unknown parameter related to surface roughness), at the cost of further simplifying the other scattering models: After all, if their power is small, a simple model for double-bounce and volume components may be sufficient; conversely, in significantly vegetated areas, improved parametric vegetation models with hybrid decomposition [22], [23] should be more conveniently used since a simple surface scattering model may be sufficient. Open questions are: which surface model to use for the case of moderately vegetated surfaces, what inversion procedure to use for soil moisture retrieval, and what quantitative criterion to use to distinguish "moderate" (or "sparse") from "significant" (or "dense") vegetation cover. This paper addresses and answers all of these three questions. It must be noted that a similar approach (i.e., simple dipole-cloud volumetric model used in the moderate vegetation case) has been recently proposed in the polarimetric decomposition technique by Lee *et al.* [35]. However, in [35], no soil moisture retrieval is proposed. In addition, in the moderate vegetation case, for the surface component the X-Bragg model is used, and the roughness parameter is heuristically retrieved by iteratively finding its smallest value that avoids the negative power problem. Conversely, we here prefer to use PTSM, which is more satisfactory from a theoretical viewpoint, is in good agreement with scattering measurements over bare soils, and allows better moisture retrieval results for bare soils [13]. In addition, we prefer the more physical approach of retrieving the roughness parameter simultaneously to soil moisture by fitting the model to data. This choice is paid by the necessity to ignore the double-bounce component; however, we believe that this is often acceptable if moderately vegetated areas are considered, at least for L-band SAR data. Accordingly, in this paper, we propose a new retrieval algorithm for moderately vegetated areas, based on the combination of the PTSM with a two-component scattering model, including surface and volume contributions. In particular, we compute all the normalized radar cross sections (NRCSs) and the copolarized correlation by using the PTSM to describe the surface scattering component, and a dipole-cloud volumetric scattering model [26], [27] to describe the volume scattering contribution arising from the vegetation layer that covers the scattering surface. We call this model "polarimetric two-scale two-component model" (PTSTCM). We then show that suitable combinations of the NRCS and copolarized correlation, which we term "modified copolarized ratio" and "modified copolarized correlation coefficient," are related only to the surface parameters (i.e., the dependence on the unknown volumetric contribution intensity cancels out). As shown in Section IV, this allows us to get a reasonable estimate of the soil moisture from L-band SAR data even in moderately vegetated areas, interested by a nonnegligible volumetric scattering contribution, but where the double-bounce scattering component is negligible. According to the considered scene, this condition may happen over a large percentage of the image pixels (see Section IV-A) or a smaller one (see Section IV-B). It is important to underline again that the use of PTSM, which predicts nonnull cross polarization for the surface scattering component, allows mitigating the known inconvenience of the FD decomposition of attributing the whole cross-polarization effect to volumetric scattering, thus overestimating this latter component and causing the "negative power problem" [28]. At variance with the usual model-based decompositions, in our method, it is not even needed that the volumetric component is preliminarily estimated before the soil moisture retrieval (see Section III-B).

The basic idea on which this paper is grounded was proposed in [42]. Here, for the first time, we provide the full detailed description of the theory (see Section II) and of the retrieval technique, including a discussion of the behavior of the method with respect to the negative power problem and a detailed sensitivity analysis (see Section III). In addition, we present an extensive analysis of the method performance by comparing obtained retrieval results to *in situ* measurements (see Section IV). To this aim, data from SMEX'03 and AGRISAR'06 campaigns available in literature are considered [43], [44]. In particular, SMEX'03 data are used to validate the method for scarcely or moderately vegetated soils (see Section IV-A), whereas the AGRISAR database, which includes data from several fields covering a period that spans all the phases of vegetation growth, is used to explore the validity range of the method in terms of vegetation conditions (see Section IV-B). Finally, we compare the results of the PTSTCM with those of available three-component methods (3CMs) employing improved volume scattering models but more simplified surface scattering ones [11], [18], [22], [23] (see Section IV-C). The main aim of this comparison is to find a quantitative criterion to adaptively select between PTSTCM and 3CM on a pixel-by-pixel basis, thus obtaining a more general method providing useful soil moisture retrieval results under a wide range of vegetation conditions (see Section IV-D).

II. Theory

As discussed in Section I, in order to get reliable soil moisture estimates not only in those areas for which the surface scattering is practically the only present scattering mechanism, we consider a two-component approach, in which the scattered field is modeled as the superposition of independent surface and volume scattering components. In particular, the former is modeled by using the PTSM [13], [19] and the vegetation layer that covers the soil surface is modeled by a cloud of randomly oriented thin cylindrical scatterers, whose scattering is described in [26] and [27]. In the following, we summarize both models and reformulate them in a way that is more suitable for subsequent description of the proposed retrieval scheme, which is introduced in Section III.

A. Surface Scattering: PTSM

According to the PTSM, a soil surface is modeled as a collection of randomly tilted rough facets: Facets' roughness represents the small-scale surface roughness, whereas facets' random slope schematizes the large-scale surface roughness. The sizes of the facets are greater than the electromagnetic wavelength and than the correlation length of the small-scale roughness, but they are much smaller than the sensor geometric resolution and than the correlation length of the large-scale

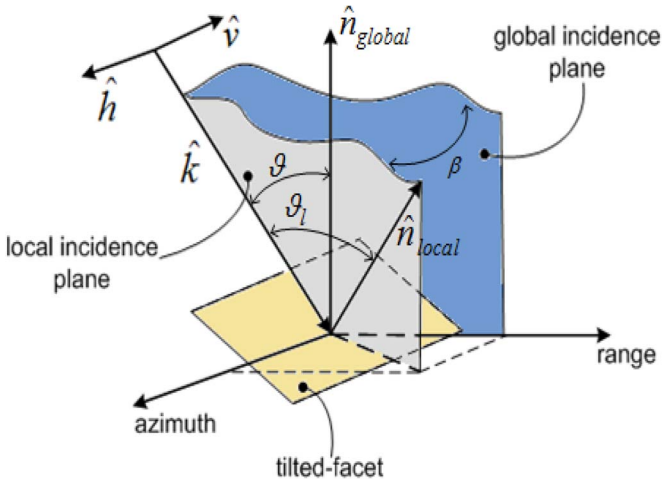

Fig. 1. Rotation of the local incidence plane and variation of the local incidence angle due to facet tilt.

roughness. Large-scale roughness and small-scale roughness are modeled as independent stochastic processes. As for the former, we assume that the facet slopes a and b along azimuth and range directions, respectively, are independent σ^2-variance Gaussian random variables, whose means represent the topographical features (if any) of the scene to be modeled [14], [19]. In the following, for the sake of simplicity, because the considered case-study areas (see Section IV) are flat, we assume zero-mean slopes. With regard to the small-scale roughness $\zeta(x, y)$, it is modeled as a zero-mean bandlimited fractional Brownian motion stochastic process [13], which is characterized by its Hurst coefficient H_t (with $0 < H_t < 1$) [13] and by its height standard deviation s_0, which is assumed small compared with the electromagnetic wavelength λ, so that it satisfies the small perturbation method (SPM), i.e., Bragg model, validity limits.

We underline that the facet random tilt gives rise to a random rotation β of the local incidence plane around the line of sight, and to a stochastic drift of the local incidence angle ϑ_l with respect to the global incidence angle ϑ (see Fig. 1). Both effects are accounted for by PTSM. In fact, the SPM expressions of the covariance matrix elements of a tilted rough facet are first considered [13], and then they are expressed in terms of facet's slopes a and b by using the well-known relations linking them to β and ϑ_l [13], [38]. Finally, the entries of the covariance matrix of the overall surface are obtained by averaging the corresponding expressions of tilted facets over a and b, after a second-order expansion around $a = 0$ and $b = 0$ [13], [19]. Their expressions can be cast in the following form (the reader interested in its algebraic derivation from the result presented in [13] and [19] is referred to the Appendix):

$$\begin{cases} \left\langle |S_{vv}|^2 \right\rangle \cong s_0^2 f_s(\varepsilon, H_t) \left(1 - \delta_V(\varepsilon)\sigma^2\right) \\ \left\langle |S_{hh}|^2 \right\rangle \cong s_0^2 f_s(\varepsilon, H_t) \left|\beta_r(\varepsilon)\right|^2 \left(1 + \delta_H(\varepsilon)\sigma^2\right) \\ \left\langle S_{hh} S_{vv}^* \right\rangle \cong s_0^2 f_s(\varepsilon, H_t) \beta_r(\varepsilon) \left(1 + \delta_{HV}(\varepsilon)\sigma^2\right) \\ \left\langle |S_{hv}|^2 \right\rangle \cong s_0^2 f_s(\varepsilon, H_t) \delta_X(\varepsilon)\sigma^2 \end{cases} \quad (1)$$

where S_{vv}, S_{hh}, and S_{hv} are the scattering matrix elements, with h and v standing for horizontal and vertical polarizations, respectively; the symbol $\langle\cdot\rangle$ stands for "statistical mean;" the asterisk $*$ stands for "complex conjugate"

$$f_s(\varepsilon, H_t) = k^4 \cos^4\vartheta \left|F_V(\vartheta;\varepsilon)\right|^2 \; W_n(2k\sin\vartheta; H_t) \quad (2)$$

$k = 2\pi/\lambda$ is the wavenumber; $W_n(\cdot)$ is the normalized power spectral density of the small-scale roughness, whose expression is reported in [13]; $F_V(\vartheta_l, \varepsilon)$ and $F_H(\vartheta_l, \varepsilon)$ are the Bragg coefficients for vertical and horizontal polarizations [13], which depend on the soil relative permittivity ε, i.e.,

$$\beta_r(\varepsilon) = \frac{F_H(\vartheta;\varepsilon)}{F_V(\vartheta;\varepsilon)} \quad (3)$$

$$\delta_X(\varepsilon) = \frac{\left|1 - \beta_r(\varepsilon)\right|^2}{\sin^2(\vartheta)} \quad (4)$$

$$\begin{cases} \delta_V(\varepsilon) = 2\mathrm{Re}\left\{\frac{1-\beta_r(\varepsilon)}{\sin^2(\vartheta)}\right\} - \frac{C_2^{VV}(\varepsilon,H_t)}{f_s(\varepsilon,H_t)} \\ \delta_H(\varepsilon) = 2\mathrm{Re}\left\{\frac{1-\beta_r(\varepsilon)}{\beta_r(\varepsilon)\sin^2(\vartheta)}\right\} + \frac{C_2^{HH}(\varepsilon,H_t)}{\left|\beta_r(\varepsilon)\right|^2 f_s(\varepsilon,H_t)} \\ \delta_{HV}(\varepsilon) = \frac{1-\beta_r(\varepsilon)}{\beta_r(\varepsilon)\sin^2(\vartheta)} - \frac{1-\beta_r^*(\varepsilon)}{\sin^2(\vartheta)} + \frac{C_2^{HV}(\varepsilon,H_t)}{\beta_r(\varepsilon) f_s(\varepsilon,H_t)} \end{cases} \quad (5)$$

$$C_2^{pq}(\varepsilon, H_t) = \frac{1}{2}\frac{\partial^2\left(W_n k^4 \cos^4\vartheta_l F_p F_q^*\right)}{\partial a^2}\bigg|_{a=b=0} + \frac{1}{2}\frac{\partial^2\left(W_n k^4 \cos^4\vartheta_l F_p F_q^*\right)}{\partial b^2}\bigg|_{a=b=0} \quad (6)$$

with p and q that can each stand for H or V.

Full analytical expressions of the derivatives in (6) are reported in [13, Appendix B]. In (1)–(6), for the sake of brevity, we have not explicitly indicated the dependence on the known global incidence angle ϑ. It is worth noting that $\beta_r(\varepsilon)$ and $\delta_{HV}(\varepsilon)$ are complex functions because, for a lossy medium, ε is a complex number and that the modulus of $\beta_r(\varepsilon)$ is smaller than unity. Conversely, $f_s(\varepsilon, H_t)$, $\delta_H(\varepsilon)$, $\delta_V(\varepsilon)$, and $\delta_X(\varepsilon)$ are real positive function. In addition, while $\beta_r(\varepsilon)$ and $\delta_X(\varepsilon)$ are rigorously independent of the small-scale roughness parameter H_t, the functions $\delta_H(\varepsilon)$, $\delta_V(\varepsilon)$, and $\delta_{HV}(\varepsilon)$ are actually also dependent on H_t [see the last terms of (5)]; however, it can be verified that this dependence tends to cancel out in the ratios of the last terms of (5), so that it is very weak and it can be neglected [13]. In the following, we will use $H_t = 0.5$ in (5). Finally, we explicitly note that PTSM reduces to the usual Bragg scattering model for $\sigma = 0$.

B. Volume Scattering: Dipole Cloud Model

With regard to the volume scattering contribution, the vegetation layer that covers the scattering surface is modeled by a cloud of randomly oriented thin cylindrical scatterers, whose covariance matrix is computed as described in [26], [27], [45], and [46]. We consider three possible probability density functions $p(\phi)$ for the dipole orientation angle ϕ, i.e., the angle, in the incident wave polarization plane, between the vertical

and the dipole directions: uniform, prevalently vertical, and prevalently horizontal distributions, i.e.,

$$p(\phi) = \frac{1}{2\pi} \text{ for } 0 \le \phi < 2\pi$$
$$p(\phi) = \frac{1}{4}|\cos\phi| \text{ for } 0 \le \phi < 2\pi$$
$$p(\phi) = \frac{1}{4}|\sin\phi| \text{ for } 0 \le \phi < 2\pi \tag{7}$$

respectively. Corresponding covariance matrix elements are [26], [27], [46]

$$\begin{cases} \langle |S_{vv}|^2 \rangle = f_v(\mathbf{u}) \\ \langle |S_{hh}|^2 \rangle = f_v(\mathbf{u}) \\ \langle S_{hh}S_{vv}^* \rangle = \frac{1}{3} f_v(\mathbf{u}) \\ \langle |S_{hv}|^2 \rangle = \frac{1}{3} f_v(\mathbf{u}) \end{cases}, \quad \begin{cases} \langle |S_{vv}|^2 \rangle = f_v(\mathbf{u}) \\ \langle |S_{hh}|^2 \rangle = \frac{3}{8} f_v(\mathbf{u}) \\ \langle S_{hh}S_{vv}^* \rangle = \frac{1}{4} f_v(\mathbf{u}) \\ \langle |S_{hv}|^2 \rangle = \frac{1}{4} f_v(\mathbf{u}) \end{cases},$$
$$\begin{cases} \langle |S_{vv}|^2 \rangle = \frac{3}{8} f_v(\mathbf{u}) \\ \langle |S_{hh}|^2 \rangle = f_v(\mathbf{u}) \\ \langle S_{hh}S_{vv}^* \rangle = \frac{1}{4} f_v(\mathbf{u}) \\ \langle |S_{hv}|^2 \rangle = \frac{1}{4} f_v(\mathbf{u}) \end{cases} \tag{8}$$

for uniform, prevalently vertical, and prevalently horizontal distributions, respectively. In (8), $f_v(\mathbf{u})$ is a function of the set of parameters $\mathbf{u}$ describing the dipole cloud. Its expression is of no concern here. Selection of the distribution depends on the vegetation type: In the absence of any information on vegetation, the uniform distribution should be selected. However, in Section IV, we will analyze the effects of different choices for the volume component description on retrieval results. Note that, here, we are assuming that volume scattering is not dominant (i.e., it is not at such a level as to determine the signum of the copolarized ratio expressed in decibels); therefore, we cannot select the volume scattering model based on the value of the measured copolarized ratio, as suggested in [27]. Moreover, as discussed in Section I, we cannot use a variable vegetation volume model as in [20]–[23] because further parameters to retrieve would appear, and this would prevent us from using the PTSM in the retrieval scheme, in order to avoid ill-posedness problems.

C. Total Scattering: PTSTCM

If the soil vegetation cover does not contain trees or other high plants, as explained in Section I, we propose to neglect double-bounce effect and consider a two-component scattering model. By assuming that, as it is reasonable, surface and volume scattering components are independent, the covariance matrix elements of a vegetated soil can be expressed as the sum of (1) and (8), so that we obtain

$$\begin{cases} \langle |S_{vv}|^2 \rangle \cong s_0^2 f_s(\varepsilon, H_t)\left(1 - \delta_V(\varepsilon)\sigma^2\right) + A f_v(\mathbf{u}) \\ \langle |S_{hh}|^2 \rangle \cong s_0^2 f_s(\varepsilon, H_t)\,|\beta_r(\varepsilon)|^2\left(1 + \delta_H(\varepsilon)\sigma^2\right) + B\, f_v(\mathbf{u}) \\ \langle S_{hh}S_{vv}^* \rangle \cong s_0^2 f_s(\varepsilon, H_t)\beta_r(\varepsilon)\left(1 + \delta_{HV}(\varepsilon)\sigma^2\right) + C\, f_v(\mathbf{u}) \\ \langle |S_{hv}|^2 \rangle \cong s_0^2 f_s(\varepsilon, H_t)\delta_X(\varepsilon)\sigma^2 + C f_v(\mathbf{u}) \end{cases} \tag{9}$$

where $A = B = 1$ and $C = 1/3$ for uniform dipole orientation; $A = 1$, $B = 3/8$, and $C = 1/4$ for prevalently vertical dipole orientation; and $A = 3/8$, $B = 1$, and $C = 1/4$ for prevalently horizontal dipole orientation.

The system (9) has four equations, of which three are real and one (the third) is complex. The parameters to retrieve are also four: ε, σ, f_v, and $s_0^2 f_s$. The first is complex, and the others are real (the last one can be considered a single parameter if s_0 and H_t do not need to be retrieved individually). Accordingly, the number of unknowns equates the number of equations, and the system is consistent (note that assuming a real dielectric constant ε, which is reasonable at microwave frequencies, the third equation also becomes real). Inclusion of a double-bounce component or of a more refined volumetric component model would introduce further unknowns; therefore, this cannot be done, unless one imposes further conditions or arbitrarily fixes one of the unknowns. For instance, by setting $\sigma = 0$, one can add a double-bounce component and recover the usual FD decomposition. A fixed nonzero value of σ can also be used. However, we believe that, in moderately vegetated areas, it is more important to better describe surface roughness by leaving σ variable than accounting for double bounce or using more refined volumetric models, such as those employed in [11], [20]–[23], [27], [29], [34], [40], [41], [47], [48]. For the same reason, we are assuming that surface scattering attenuation due to vegetation is the same at all polarizations, so that the corresponding attenuation factor can be included in the f_s function and hence be ignored in the soil moisture retrieval procedure.

We explicitly note that expressions in (9) ensure that both the surface and volume component covariance matrices are positive semi-definite, provided that the retrieved values of f_v and $s_0^2 f_s$ are nonnegative. A full discussion on this issue can be found in Section III. Here, we only want to emphasize that, by employing usual model-based decompositions, the volumetric component is computed as

$$f_v(\mathbf{u}) = \frac{\langle |S_{hv}|^2 \rangle}{C} \tag{10}$$

therefore attributing the whole cross-polarization effect to volumetric scattering, whereas the use of the last equation in (9) leads to

$$f_v(\mathbf{u}) = \frac{\langle |S_{hv}|^2 \rangle - s_0^2 f_s(\varepsilon, H_t)\delta_X(\varepsilon)\sigma^2}{C} \le \frac{\langle |S_{hv}|^2 \rangle}{C} \tag{11}$$

so that the problem of overestimating the volumetric component is certainly mitigated by our model.

III. Retrieval Method

A. Description of the Method

Previously developed PTSM-based retrieval methods for bare soils were based on the combined use of copolarized (copol) and cross-polarized (crosspol) ratios [13] or of the copolarized ratio and copolarized correlation (corr) coefficient

[19]. The copol and crosspol ratios and corr coefficient are defined as follows:

$$\begin{cases} \text{Copol} = \frac{\langle |S_{hh}|^2 \rangle}{\langle |S_{vv}|^2 \rangle} \\ \text{Crosspol} = \frac{\langle |S_{hv}|^2 \rangle}{\langle |S_{vv}|^2 \rangle} \\ \text{Corr} = \frac{|\langle S_{hh} S_{vv}^* \rangle|}{\sqrt{\langle |S_{hh}|^2 \rangle \langle |S_{vv}|^2 \rangle}}. \end{cases} \tag{12}$$

Their use is motivated by the fact that, according to PTSM, they do not depend on small-scale roughness parameters s_0 and H_t, and they only depend on the soil relative permittivity ε and on the standard deviation σ of the large-scale roughness slopes. In fact, by using (1) in (12), expanding in Taylor series with respect to σ, and retaining terms up to the second order, we obtain

$$\begin{cases} \text{Copol} \cong |\beta_r(\varepsilon)|^2 \left(1 + \delta_{\text{copol}}(\varepsilon)\sigma^2\right) \\ \text{Crosspol} \cong \delta_X(\varepsilon)\sigma^2 \\ \text{Corr} \cong 1 - \delta_{\text{corr}}(\varepsilon)\sigma^2 \end{cases} \tag{13}$$

where

$$\begin{aligned} \delta_{\text{copol}}(\varepsilon) &= \delta_H(\varepsilon) + \delta_V(\varepsilon) \\ \delta_{\text{corr}}(\varepsilon) &= \frac{1}{2}\delta_H(\varepsilon) - \frac{1}{2}\delta_V(\varepsilon) - \text{Re}\left\{\delta_{HV}(\varepsilon)\right\} \end{aligned} \tag{14}$$

are real positive functions. Accordingly, if we neglect the imaginary part of ε as it is reasonable for usual soils at microwave frequencies [49] (or also if we assume that there is a relationship relating real and imaginary parts of ε at the considered frequency, as in [49]), it is possible to retrieve σ and ε from measured copol and crosspol ratios [13] or, equivalently, from measured copol ratio and corr coefficient [19]. Soil moisture can be then evaluated from ε by using one of the available semi-empirical mixing models [49]–[51].

However, if a nonnegligible volumetric scattering component due to vegetation is present, from (9), it is clear that the ratios in (12) are no longer independent of small-scale roughness, and they are of course also dependent on the volumetric component. Therefore, it is expected that in this case the methods of [13] or [19] lead to wrong retrieval results.

Here, we propose to properly combine the polarimetric channels in such a way to cancel out the dependence on f_v and to recover independence from small-scale roughness. In particular, we define a "modified copolarized ratio" and a "modified copolarized correlation coefficient" as follows:

$$\begin{cases} \text{Copol}_{\text{mod}} = \frac{\langle |S_{hh}|^2 \rangle - \frac{B}{C}\langle |S_{hv}|^2 \rangle}{\langle |S_{vv}|^2 \rangle - \frac{A}{C}\langle |S_{hv}|^2 \rangle} = \frac{\text{Copol} - \frac{B}{C}\text{Crosspol}}{1 - \frac{A}{C}\text{Crosspol}} \\ \text{Corr}_{\text{mod}} = \frac{\left|\langle S_{hh} S_{vv}^* \rangle - \langle |S_{hv}|^2 \rangle\right|}{\sqrt{\left(\langle |S_{hh}|^2 \rangle - \frac{B}{C}\langle |S_{hv}|^2 \rangle\right)\left(\langle |S_{vv}|^2 \rangle - \frac{A}{C}\langle |S_{hv}|^2 \rangle\right)}}. \end{cases} \tag{15}$$

In fact, the use of (9) in (15) shows that the terms containing f_v cancel out in the numerator and denominator of both ratios in (15). In particular, by using (9) in (15), expanding in Taylor series with respect to σ, and retaining terms up to the second order, we obtain

$$\begin{cases} \text{Copol}_{\text{mod}} \cong |\beta_r(\varepsilon)|^2 \left(1 + \delta_{\text{copol}}(\varepsilon)\sigma^2 + \delta'_{\text{copol}}(\varepsilon)\sigma^2\right) \\ \text{Corr}_{\text{mod}} \cong 1 - \delta_{\text{corr}}(\varepsilon)\sigma^2 + \delta'_{\text{corr}}(\varepsilon)\sigma^2 \end{cases} \tag{16}$$

where

$$\begin{aligned} \delta'_{\text{copol}}(\varepsilon) &= \frac{\delta_X(\varepsilon)}{C}\left(A - \frac{B}{|\beta_r(\varepsilon)|^2}\right) \\ \delta'_{\text{corr}}(\varepsilon) &= \frac{\delta_X(\varepsilon)}{2C}\left(A + \frac{B}{|\beta_r(\varepsilon)|^2} - \text{Re}\left\{\frac{2C}{\beta_r(\varepsilon)}\right\}\right). \end{aligned} \tag{17}$$

Both $\delta'_{\text{copol}}(\varepsilon)$ and $\delta'_{\text{corr}}(\varepsilon)$ are real functions. The signum of $\delta'_{\text{corr}}(\varepsilon)$ depends on the value of $\beta_r(\varepsilon)$, and the same holds for the signum of $\delta'_{\text{copol}}(\varepsilon)$for prevalently vertical dipole orientation. However, for prevalently horizontal ($A = 3/8$, $B = 1$) and uniform ($A = B = 1$) dipole orientations, by recalling that $|\beta_r(\varepsilon)| < 1$, it is easy to verify that $\delta'_{\text{copol}}(\varepsilon)$ is negative. Finally, note that the modified correlation coefficient is not a true correlation coefficient, so that it is not restricted to be smaller than unity.

Equations (15)–(17) can be used for the retrieval of σ and ε from the measured modified copol ratio and modified corr coefficient exactly in the same way as (12)–(14) are used for the retrieval of σ and ε from the measured copol ratio and corr coefficient. In fact, in both cases, it is possible to build up charts (see Fig. 2) or numerical lookup tables of (possibly modified) copol–corr loci parameterized by the dielectric constant ε (or, equivalently, the soil moisture content m_v) and the large-scale roughness rms slope σ. Accordingly, the same automatic estimation algorithm as in [13] and [19] can be used, with the same advantages: it is a physically based inversion approach, processing time is very short, and no preliminary model calibration phase is needed [19]. We explicitly note here that the elements of the covariance matrix are computed by averaging neighboring pixels over windows of size such that a very high equivalent number of looks (ENL), on the order of 100, is obtained. Accordingly, the resolution cell size of the final soil moisture maps is one order of magnitude larger than the size of the SAR system single-look resolution cell.

It must be mentioned that formulations similar to those of (12)–(14) or (15)–(17) can be also obtained by using the elements of the polarimetric coherency, rather than covariance, matrix. The coherency matrix is sometimes preferred because its elements have a more direct physical interpretation (see, e.g., [10] and [11]). However, we here prefer the formulation in terms of the polarimetric covariance matrix mainly because it was verified in [13], and it was confirmed here that second-order expansions of copolarized ratio and correlation coefficient (and their modified versions) with respect to large-scale roughness surface slopes have a wider range of validity (in terms of σ) if one uses the elements of the covariance matrix than the elements of the coherency matrix. In particular, (13) and (16) can be safely employed for values of σ smaller than about 0.4 (corresponding to an rms slope of about 21°), so that $\delta_{\text{copol}}(\varepsilon)\sigma^2$, $\delta_{\text{corr}}(\varepsilon)\sigma^2$, $\delta'_{\text{copol}}(\varepsilon)\sigma^2$, and $\delta'_{\text{corr}}(\varepsilon)\sigma^2$ are all small compared with one [13], [19]. In addition, the coherency matrix copolarized ratio is very sensitive to the presence of a double-bounce scattering component (due to the presence of the difference of HH and VV channels at its numerator): This is an advantage in general, but it may be a problem if the double-bounce component is not included in the model, as in our case.

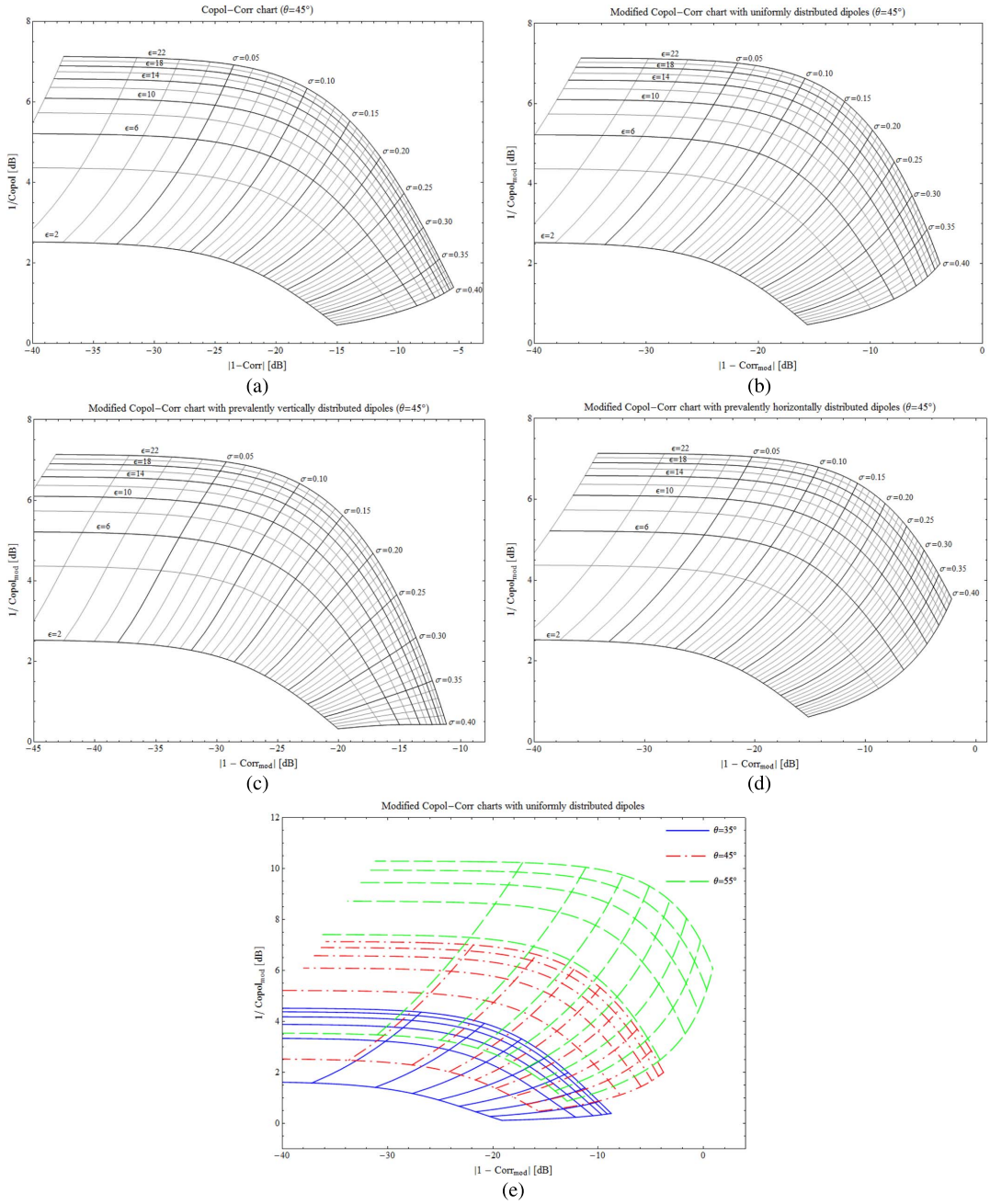

Fig. 2. (a) PTSM-based copol–corr and (b)–(d) PTSTCM-based modified copol–corr charts for $H_t = 0.5$ and $\vartheta = 45°$, with (b) uniformly, (c) prevalently vertically, and (d) prevalently horizontally distributed dipoles, and (e) for different values of the incidence angle, with uniformly distributed dipoles. In the graphs, ε represents the relative permittivity, and σ is the rms slope of the large-scale roughness.

A block scheme of the algorithm is shown in Fig. 3. Note that no retrieval result is obtained if the measured SAR data lead to values of ε smaller than 2.5 and larger than 40 or to values of σ larger than 0.4, or if at least one of the factors under the square root in the second of (15) is nonpositive.

B. Reduction of the "Negative Power" Problem

At variance with usual model-based decompositions, in our method, the volumetric component is not preliminarily estimated before the soil moisture retrieval: In fact, as explained earlier, soil moisture and soil roughness are retrieved with no necessity to evaluate the volume f_v and surface $s_0^2 f_s$ contribution intensities. However, if desired, of course, the latter can be estimated once soil moisture (m_v) (or better, the dielectric constant ε) and soil roughness (σ) parameters have been retrieved. This can be done by solving the fourth of (9) for f_v and substituting in the first of (9), thus obtaining

$$\begin{aligned} s_0^2 f_s(\varepsilon, H_t) &= \frac{\left\langle |S_{vv}|^2 \right\rangle - \frac{A}{C}\left\langle |S_{hv}|^2 \right\rangle}{\left(1 - \delta_V(\varepsilon)\sigma^2 - \frac{A}{C}\delta_X(\varepsilon)\sigma^2\right)} \\ &\cong \left(\left\langle |S_{vv}|^2 \right\rangle - \frac{A}{C}\left\langle |S_{hv}|^2 \right\rangle\right) \\ &\quad \times \left(1 + \delta_V(\varepsilon)\sigma^2 + \frac{A}{C}\delta_X(\varepsilon)\sigma^2\right) \end{aligned} \tag{18}$$

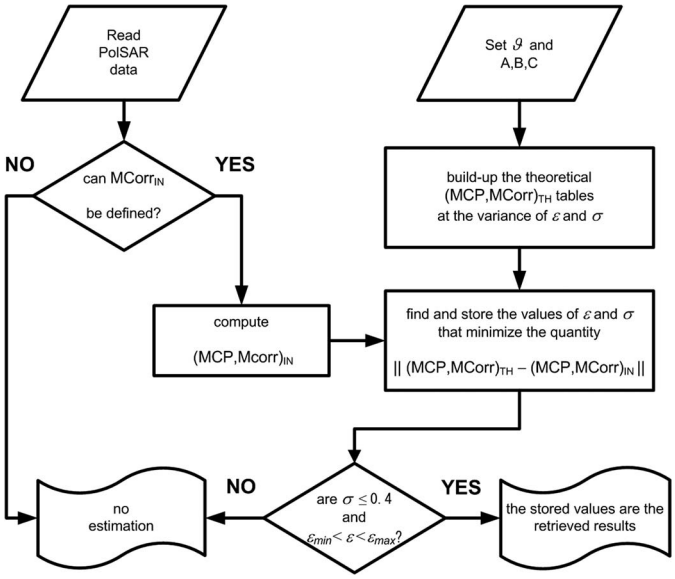

Fig. 3. Block scheme of the retrieval procedure. $\mathrm{MCP_{IN}}$ and $\mathrm{MCorr_{IN}}$ are the input modified copolarized ratio and modified correlation coefficient measured from SAR data, whereas $\mathrm{MCP_{TH}}$ and $\mathrm{MCorr_{TH}}$ are their theoretical values, computed from (16) and (17). Finally, $\varepsilon_{\min} = 2.5$ and $\varepsilon_{\max} = 40$.

$$f_v(\mathbf{u}) = \frac{\langle |S_{hv}|^2 \rangle - s_0^2 f_s(\varepsilon, H_t)\delta_X(\varepsilon)\sigma^2}{C} \cong \frac{\langle |S_{hv}|^2 \rangle - \left(\langle |S_{vv}|^2 \rangle - \frac{A}{C}\langle |S_{hv}|^2 \rangle\right)\delta_X(\varepsilon)\sigma^2}{C}. \quad (19)$$

In (18) and (19), the terms of order higher than two with respect to σ have been neglected.

In order to avoid the negative power problem for the surface component, it is sufficient that $s_0^2 f_s$ is nonnegative. In view of (18), the following condition must be fulfilled by data:

$$\langle |S_{hv}|^2 \rangle_{|\zeta,a,b} \leq \frac{C}{A}\langle |S_{vv}|^2 \rangle_{|\zeta,a,b}, \text{i.e.,} \quad \text{Crosspol} \leq \frac{C}{A}. \quad (20)$$

This condition is usually not violated in moderately vegetated flat areas, which are of interest for our method. In Section IV-A and B we show that, according to the considered scene, the percentage of pixels violating this condition, i.e., facing the negative power problem, may vary from 2% to about 20%. In addition, it is important to note that if condition (20) is violated, then no result is provided by our PTSTCM-based algorithm (see Fig. 3) because, in this case, the modified correlation coefficient cannot be defined (the argument of the square root at the denominator becomes negative). This may happen in very vegetated areas, where ignoring double bounces and using our simple vegetation model are not adequate, and in areas with significant topography if the latter is not compensated for as discussed in Section I. We can then conclude that, when the soil moisture retrieval is obtained by PTSTCM, the surface component certainly has a positive semi-definite (positive definite) covariance matrix.

However, since, in our case, the surface component is estimated first, nonnegativity of the retrieved volume component power must be checked. In order to avoid the negative power problem for the volume component, f_v must be nonnegative, so that, in view of (19), the following condition must be satisfied by σ^2:

$$\sigma^2 \leq \frac{\langle |S_{hv}|^2 \rangle_{|\zeta,a,b}}{\delta_X(\varepsilon)\left(\langle |S_{vv}|^2 \rangle_{|\zeta,a,b} - \frac{A}{C}\langle |S_{hv}|^2 \rangle_{|\zeta,a,b}\right)} = \frac{\text{Crosspol}}{\delta_X(\varepsilon)\left(1 - \frac{A}{C}\text{Crosspol}\right)}. \quad (21)$$

We have verified that this condition is satisfied in the large majority of cases in which our method leads to a retrieval result. For instance, in the examples considered in Section IV, condition (21) is satisfied in the 95% of "retrieved" pixels. In any case, the negative power problem can be completely avoided if the retrieved value of σ is chosen as the minimum between the value obtained by PTSTCM and the value given by the right-hand side of (21).

Finally, it is useful to underline that, even in the cases in which nonnegativity of power is guaranteed, the proposed method is not expected to provide reliable results when the double-bounce component is not negligible or even dominant. The latter situation can be easily identified from SAR data by using the criterion suggested in [26], based on the signum of the real part of the "vegetation-corrected" correlation: Accordingly, results obtained in pixels for which $\mathrm{Re}\{\langle S_{hh}S_{vv}^* \rangle\} - \langle |S_{hv}|^2 \rangle < 0$ must be discarded as they are not reliable. In Section IV-A and B we show that, according to the considered scene, the percentage of pixels for which this happens may vary from 4% to about 70%.

C. Sensitivity Analysis

The proposed method is clearly not affected by absolute calibration errors, which cancel out in the ratios of (15); however, channel power and phase imbalance, channel crosstalk, speckle, and thermal noise, are in principle all sources of errors on the measurement of modified copolarized ratio and correlation coefficient, and hence on soil moisture retrieval. Given an error on modified copol and corr, its effect on the retrieval of ε and hence of m_v can be evaluated by using the charts of Fig. 2. As we will see later here, errors on the order of ± 0.5 dB or less on modified copol and on the order of ± 1 dB or less on modified corr can be expected for most SAR systems. Based from the charts in Fig. 2(b)–(d), we can verify that, if $\vartheta = 45°$, a $\pm$0.5-dB error on modified copol causes a small error on ε, on the order of ± 1 (corresponding to about ± 2 vol.% soil water content), for small values of ε (e.g., $\varepsilon < 6$, i.e., $m_v < 10$ vol.%), and an increasing error for increasing values of ε. For $\varepsilon = 20$ (i.e., m_v about 30 vol.%), an error on the order of about ± 6 is obtained (corresponding to about ± 7 vol.% soil water content). In both cases, maximum relative error on m_v is on the order of 20%. Conversely, for small values of σ (e.g., $\sigma < 0.1$), a $\pm$1-dB error on corr has practically no effect on the retrieval of ε, whereas for large values of σ (e.g., $\sigma > 0.2$), the effects of errors on corr are of the same order as those of errors on copol. The chart in Fig. 2(e) shows that the effects on soil moisture

retrieval of errors on modified copol and corr increase for smaller incidence angle and decrease for larger incidence angle.

Let us now consider the effect of channel power imbalance on modified copol and corr. For simplicity, let us assume that the same power imbalance α between H and V channels is present on both the transmitting and the receiving chains, so that the measured values are related to true ones by

$$\begin{cases} \hat{\text{Copol}} = \alpha^2 \text{Copol} \\ \hat{\text{Crosspol}} = \alpha\, \text{Crosspol} \\ \hat{\text{Corr}} = \text{Corr}. \end{cases} \tag{22}$$

By using (22) in (15), we get

$$\begin{cases} \hat{\text{Copol}}_{\,\text{mod}} = \alpha^2 \text{Copol}_{\,\text{mod}} \dfrac{\left(1+\frac{\frac{B}{C}\langle |S_{hv}|^2\rangle\left(1-\frac{1}{\alpha}\right)}{\langle |S_{hh}|^2\rangle - \frac{B}{C}\langle |S_{hv}|^2\rangle}\right)}{\left(1+\frac{\frac{A}{C}\langle |S_{hv}|^2\rangle(1-\alpha)}{\langle |S_{vv}|^2\rangle - \frac{A}{C}\langle |S_{hv}|^2\rangle}\right)} \\ \hat{\text{Corr}}_{\,\text{mod}} \\ \quad = \text{Corr}_{\,\text{mod}} \dfrac{1}{\sqrt{\left(1+\frac{\frac{B}{C}\langle |S_{hv}|^2\rangle\left(1-\frac{1}{\alpha}\right)}{\langle |S_{hh}|^2\rangle - \frac{B}{C}\langle |S_{hv}|^2\rangle}\right)\left(1+\frac{\frac{A}{C}\langle |S_{hv}|^2\rangle(1-\alpha)}{\langle |S_{vv}|^2\rangle - \frac{A}{C}\langle |S_{hv}|^2\rangle}\right)}}. \end{cases} \tag{23}$$

By noting that the quantities in the large parentheses in (23) are approximately unitary because $\alpha \cong 1$ and the cross-polarized power is often much smaller than copolarized one (at least when our model is valid), we can conclude that the effect of power imbalance on a modified copol ratio is on the order of α^2, whereas its effect on the modified correlation coefficient is negligible. For modern SAR systems, it is reasonable to assume that α^2 is on the order of ± 0.5 dB or less. For instance, the requirement on relative calibration error for DLR E-SAR and F-SAR systems is that it must be smaller than 1 dB [52], and the declared α^2 of ALOS-PALSAR 2 is 1.0143, i.e., 0.062 dB [53].

Let us now move to consider the effect of a phase imbalance $\Delta\phi$, which only affects the HH-VV correlation:

$$\left\langle \hat{S}_{hh}\hat{S}_{vv}^* \right\rangle = \langle S_{hh}S_{vv}^* \rangle \exp(j\Delta\phi). \tag{24}$$

The modified copolarized ratio is not affected by phase imbalance, whereas for the modified correlation coefficient, by using (24) in the second of (15), we get

$$\begin{aligned} \hat{\text{Corr}}_{\,\text{mod}} &= \frac{\left|\langle S_{hh}S_{vv}^*\rangle \exp(j\Delta\phi) - \langle |S_{hv}|^2\rangle\right|}{\left|\langle S_{hh}S_{vv}^*\rangle - \langle |S_{hv}|^2\rangle\right|} \\ &\cong \text{Corr}_{\,\text{mod}} \left(1 - \text{Im}\left\{\frac{\langle S_{hh}S_{vv}^*\rangle}{\langle S_{hh}S_{vv}^*\rangle - \langle |S_{hv}|^2\rangle}\right\}\Delta\phi\right) \end{aligned} \tag{25}$$

where terms of order higher than one with respect to $\Delta\phi$ are neglected. Therefore, by considering that the imaginary part of the copolarized correlation is small at microwave frequencies, that cross-polarized power is usually significantly smaller than the copolarized correlation modulus, and that for modern SAR system phase imbalance is always smaller (in absolute value) than about $\pi/20$ rad, we can conclude that the phase imbalance effect is negligible. For instance, by assuming that the imaginary part in (25) is 0.1, and phase imbalance is $\pi/20$ rad, we obtain an error of 0.07 dB on the modified correlation coefficient.

With regard to channel crosstalk, in modern SAR systems, it is smaller (sometimes much smaller) than -25 dB, so that it only affects the cross-polarized ratio, and only when the latter is so low that it has no impact on modified copol and corr [see (15)].

Let us now move to consider the effect of speckle on polarimetric SAR data statistics, which was studied in detail in [54]. Due to speckle, the channel intensity ratios have random fluctuations. However, considerations reported in [54] and the use of the first part of (15) lead to the conclusion that, for an ENL greater than about 70, the uncertainty on the modified copol is always smaller than 0.5 dB, and usually (i.e., when the cross-polarized ratio is small), it is negligible. The situation is different with regard to the speckle effect on the correlation coefficient. In this case, the estimated correlation coefficient has both a bias and an uncertainty [54]. For an ENL larger than about 70, the bias is negligible, particularly for high values of the correlation coefficient. Conversely, even for an ENL on the order of 70, the uncertainty on the correlation coefficient is between 0.5 and 1 dB [54]. Accordingly, in view of the second part of (15), we can conclude that, for ENL > 70, the uncertainty on the modified corr is on the order of 1 dB or smaller.

Finally, let us consider the effect of the receiver thermal noise, modeled as a zero-mean complex additive white Gaussian noise. We also assume that the covariance matrix elements are evaluated by spatially averaging over a number of adjacent pixels on the order of 100 (i.e., over an about 10×10 pixel window), so that spatial average is an accurate estimate of statistical mean. Finally, we reasonably assume that the power values n^2 of noise on all channels are equal, that noise and signal are independent, and that noises on HH and VV channels are independent. By using these assumptions and employing (15), we have that noisy estimates of modified copol and corr are related to the true values by

$$\begin{cases} \hat{\text{Copol}}_{\,\text{mod}} = \text{Copol}_{\,\text{mod}} \dfrac{\left(1+\frac{\left(1-\frac{B}{C}\right)n^2}{\langle |S_{hh}|^2\rangle - \frac{B}{C}\langle |S_{hv}|^2\rangle}\right)}{\left(1+\frac{\left(1-\frac{A}{C}\right)n^2}{\langle |S_{vv}|^2\rangle - \frac{A}{C}\langle |S_{hv}|^2\rangle}\right)} \\ \hat{\text{Corr}}_{\,\text{mod}} \\ \quad = \text{Corr}_{\,\text{mod}} \dfrac{1}{\sqrt{\left(1+\frac{\left(1-\frac{B}{C}\right)n^2}{\langle |S_{hh}|^2\rangle - \frac{B}{C}\langle |S_{hv}|^2\rangle}\right)\left(1+\frac{\left(1-\frac{A}{C}\right)n^2}{\langle |S_{vv}|^2\rangle - \frac{A}{C}\langle |S_{hv}|^2\rangle}\right)}}. \end{cases} \tag{26}$$

Based on (26), we obtain that if the SNR on the HH and VV channels is larger than 20 dB, then the error on modified copol and corr is negligible (less than 0.1 dB). As an exception to this, a critical situation may exist if the HV channel power is about C/B times the HH one or C/A times the VV one [see (26)]; however, this may happen only in extremely vegetated areas, where our model is not valid. Note that for low values of the HV scattering, the HV channel may be strongly affected by noise, but this does not affect modified copol and corr parameters as long as the SNR on copolarized channels is high enough. In view of the scattering measurements reported in [2], [6], the

20 dB requirement on SNR for copolarized channels calls for a noise equivalent sigma zero (NESZ) on the order of -35 dB at the L-band and over small-roughness bare soils. Values of NESZ on the order of -25 dB (i.e., HH and VV SNR on the order of 10 dB for small-roughness bare soils) would imply errors on the order of 0.5–1 dB for small-roughness bare soils, and much smaller errors for rough and/or vegetated soils. Such requirements are met by most modern SAR systems.

In conclusion, the performed analysis shows that, for most SAR systems and for many observed scenarios, errors on the order of ± 0.5 dB or less can be expected on modified copol, usually mainly due to relative calibration errors, and errors on the order of ± 1 dB or less can be expected on modified corr, usually mainly due to speckle. This leads to maximum relative errors on soil moisture on the order of 20%. Accordingly, higher errors should be always mainly attributed to model inaccuracy.

IV. Retrieval Results

In the following, we evaluate the soil moisture retrieval results obtained with SAR data acquired in the framework of the 2003 SMEX'03 and the 2006 AgriSAR campaigns. With regard to the former, the data set consists of L-band data acquired on several close dates by the JPL AIRSAR sensor over the Little Washita basin [43]; with regard to the latter, we use L-band SAR data acquired by the DLR airborne experimental SAR (E-SAR) system in the site of Demmin in northern Germany, during one whole vegetation cycle [44]. In both cases, simultaneously to SAR acquisitions, on-field measurements of the volumetric soil moisture were performed, allowing for meaningful comparisons of obtained retrieval results with ground-truth data. It must be noted that both method estimates and *in situ* measurements, relevant to each single field and for each single acquisition, show large standard deviations, often of the same order of mean values. Accordingly, for each field and at each acquisition date, we compare average values of retrieved and *in situ* measured soil moisture.

We do not consider higher frequency sensors (at C-band or X-band) because it is expected that, at those frequency, in the presence of even medium or moderate vegetation, volume scattering is dominant. Finally, we also present a comparison of our results with those obtained on the same AgriSAR data set using three-component models that include also double-bounce scattering. Based on this comparison, we propose a simple method to adaptively and automatically (i.e., based on measured data) select between PTSTCM and 3CM on a pixel-by-pixel basis.

A. SMEX'03

Here, we consider L-band AIRSAR data acquired on several days during one week of July 2003, in the framework of the SMEX'03 measurement campaign in the Little Washita basin [43]. They refer to a scene for which the proposed PTSTCM is expected to apply because it mainly consists of agricultural fields with a scarce to moderate vegetation cover. Accordingly, these data are used to compare the retrieval results obtained without vegetation compensation and with the compensation method based on the random uniformly distributed dipole orientation model. In fact, we expect that this simple volumetric component model is appropriate for this kind of vegetation (see also Section IV-B, where this is experimentally confirmed).

SMEX'03 AIRSAR data are stored in compressed Stokes matrix format [43]. From the Stokes matrix elements, all the elements of the covariance (needed by our methods) and of the coherency matrices can be easily obtained [45], [46]. Here, we focus on the region of about 8×8 km^2 surrounding the measurement sites labeled in [43] as LW20, LW21, LW22, LW27, LW28, and LW29 [see Fig. 4(a)], for which the soil moisture was measured *in situ* at the same times of the AIRSAR acquisitions. In particular, *in situ* measured volumetric soil moisture in the top 6-cm layer are available. More details on the ground-truth data acquisition are provided in [43].

Based on photos and descriptions available in [43], the considered test sites can be labeled as scarcely (LW21, LW22) to moderately (all other sites) vegetated soils. The estimation procedure has been performed on this data set, leading to the estimation maps of the volumetric soil moisture (an example of which, without and with vegetation compensation, is depicted in Fig. 4(c) and (d), obtained from the soil permittivity maps through the Hallikainen mixing model[1] [49] (average values of percentages of sand and clay can be derived from data in [43], and they are about 45% and 13%, respectively). Pauli decomposition maps, an example of which is reported in Fig. 4(b), confirm that surface scattering is dominant in most of the scene, and that this dominance is stronger for fields LW21 and LW22 than for the other fields. In this scenario, the overall percentage of pixels for which retrieval is obtained (the "inversion rate") is 63% and 66% for the uncompensated and compensated cases (with uniformly distributed dipoles' orientations), respectively. In addition, in the six fields considered in this paper, the percentage of pixels suffering from the negative power problem (i.e., for which condition (20), with C/A $= 1/3$, is not fulfilled) is 2% [see Fig. 4(e)], and the percentage of pixels for which double bounce is dominant (i.e., for which the real part of the vegetation-corrected correlation is negative) is 4%.

The obtained soil moisture estimates are compared with the available ground truth. In particular, in Fig. 5(a), the scatterplot of the results obtained through the inversion procedure of [19] (i.e., without vegetation compensation) are reported, whereas in Fig. 5(b) those obtained via the proposed vegetation compensation approach (with uniformly distributed dipoles' orientations) are shown. In the former case, the mean error (ME) is equal to 6.9 vol.% with an error standard deviation (SDE) of 3.7 vol.% (so that the rmse is 7.8), and the correlation coefficient (ρ) is equal to 0.74. In case of vegetation compensation, SDE and ρ are unchanged, but the ME decreases to ME $= 1.2$ vol.% (so that the rmse decreases to 3.9). In fact, looking at the plots in Fig. 5, the improvement with respect to the ME is evident. This figure also shows that the main effect on PTSM soil moisture retrieval of noncompensated vegetation is an overestimation.

[1]If soil mixture is not known, the Topp model can be used [50]. We have verified that the use of the Topp model only leads to a small difference in the retrieval results that does not substantially change the conclusion of this paper. The same holds if the updated version of the Hallikainen model provided by Mironov [51] is employed.

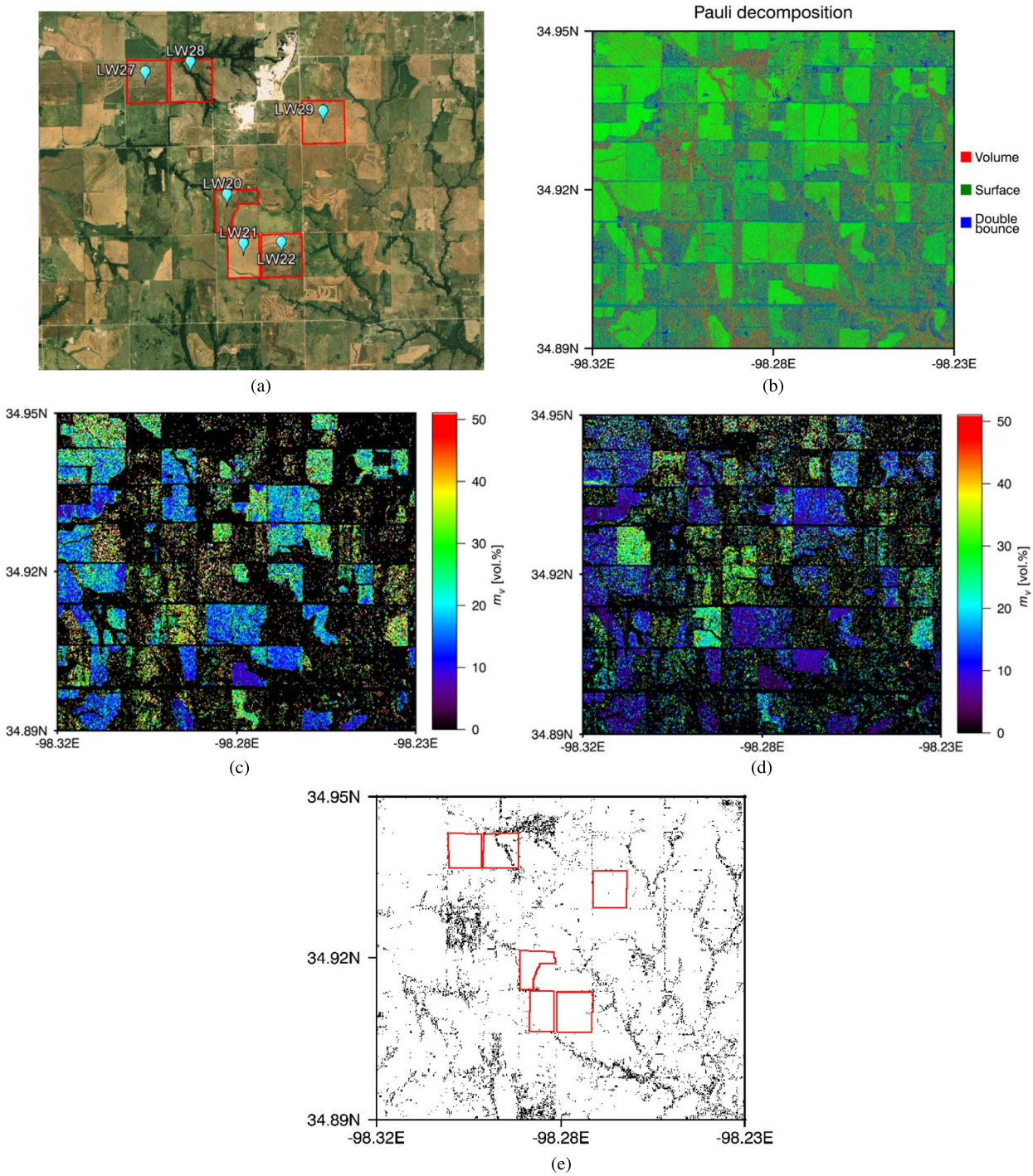

Fig. 4. (a) Optical image of the considered scene with indication of *in situ* measurements. (b) Pauli decomposition. (c) Soil moisture map with no vegetation compensation and (d) soil moisture map with vegetation compensation pertinent to the AIRSAR acquisition of July 3, 2003 (black pixels: parameter not retrieved). (e) Map reporting in black the pixels experiencing the negative power problem. The borders of the considered fields appear in red in (a) and (e). The area is about 8000 m $\times$ 8000 m wide.

This is because the presence of vegetation causes a slight increase in the copol ratio and a significant decrease in the correlation coefficient; accordingly, the point representing SAR data on the graph of Fig. 2(a) moves toward the right (and only slightly downward), so that the retrieved ε increases. It is also interesting to note that, as expected, this soil moisture overestimation is smaller for the less vegetated fields LW21 and LW22 (ME $= 5$ vol.%) than for the other considered fields (ME $=$ 8 vol.%), and that it is almost canceled by vegetation compensation for both groups of fields (ME about -1 and 1.5 vol.%, respectively).

In summary, here, we have shown that, in the favorable scenario of agricultural fields with a scarce to moderate vegetation cover, the PTSTCM (i.e., the vegetation-corrected PTSM) allows to properly correct the PTSM soil moisture overestimation caused by the presence of vegetation.

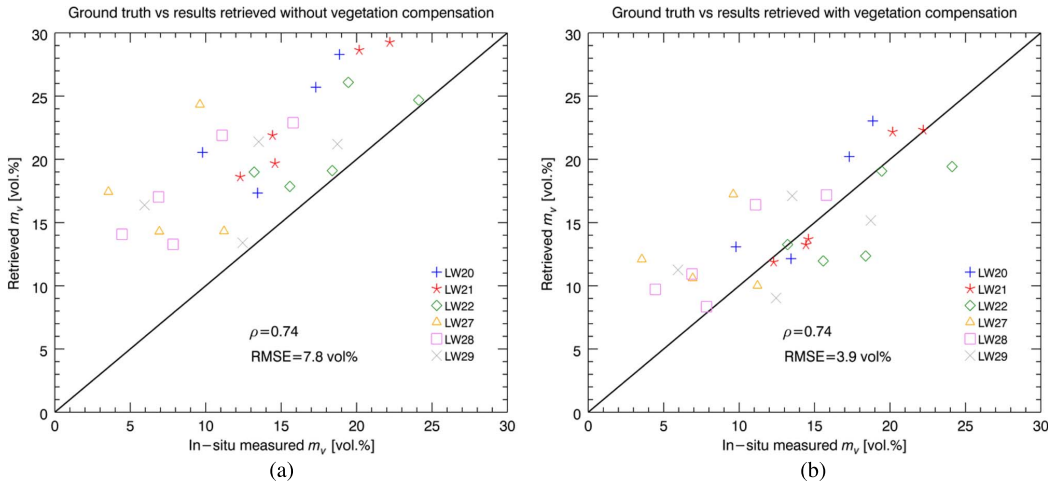

Fig. 5. Scatterplots of the retrieval results versus measured ground truth. (a) Without vegetation compensation (PTSM). (b) With vegetation compensation (PTSTCM).

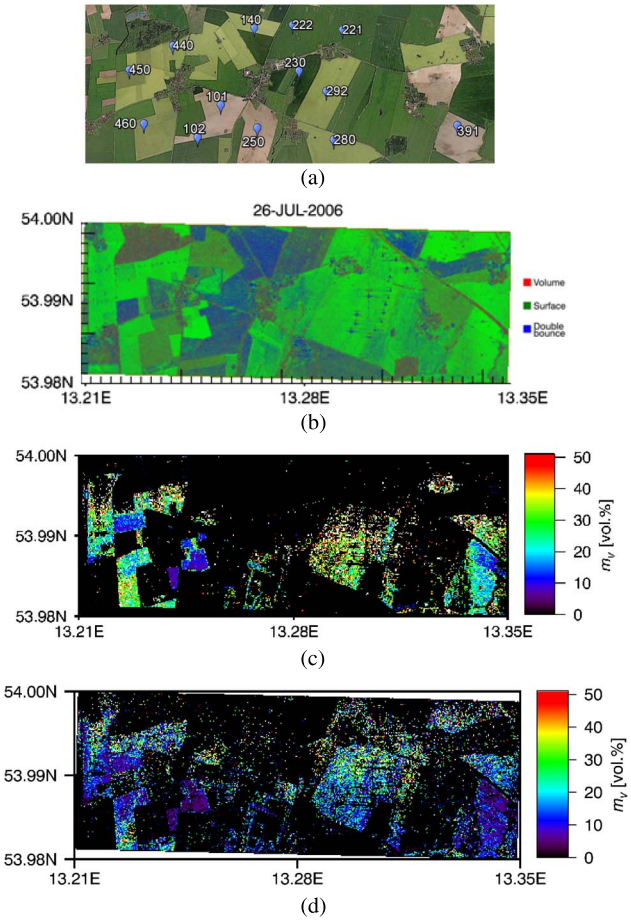

Fig. 6. (a) Optical image of the considered scene, with indication of *in situ* measurements. (b) Pauli decomposition. Soil moisture map (c) without vegetation compensation and (d) with "uniform" vegetation compensation pertinent to the E-SAR acquisition of July 26, 2006 (black pixels: parameter not retrieved). The area is about 8500 m × 3000 m wide.

B. AgriSAR

Here, we consider L-band SAR data acquired by the DLR airborne experimental SAR (E-SAR) system over the site of Demmin in northern Germany, during the whole vegetation growth cycle in the year 2006 [44]. They refer to an agricultural scenario with several different crop types [see Fig. 6(a)], whose conditions significantly change from the times of the first acquisitions to those of the latest ones, moving from scarcely, to moderately, and finally to very vegetated fields. It is then expected that the proposed PTSTCM can be only applied to the first acquisitions; however, we here force application to all acquisitions, to explore the validity range of the method. In addition, we want to compare results obtained employing different volume scattering models (i.e., the different kinds of vegetation compensation).

In the framework of the AgriSAR campaign, in correspondence with SAR acquisitions, a wide set of ground data was collected, regarding vegetation phenology, terrain conditions, precipitations, and volumetric soil moisture [44]. In particular, the soil water content was measured with different techniques (i.e., time-domain reflectometry, and gravimetric and capacitive measurements) and different time-sampling scenarios (intensive campaigns over many fields, weekly measures on a limited set of fields, and via continuous measurements stations over few fields). These measurements have been used as reference ground truth in our experiment. The area is characterized by altitude variations of less than 50 m, with very small slopes. Several crop types are present, and in particular, in this paper, we consider sugar beet, wheat, barley, rape, and corn. An example of Pauli decomposition map is provided in Fig. 6(b), and it shows that, in this scenario, a variety of dominant scattering mechanisms are present. In addition, this situation significantly varies with time, according to the vegetation evolution.

The retrieval procedures are applied on the available E-SAR geocoded L-band quad-polarimetric images, after application of a spatial multilook leading to a final pixel spacing of 20 m × 20 m (corresponding to a number of looks larger than 100, and to a minimum number of pixels per field equal to about 350). The estimates of ε and σ are obtained following both the procedure described in [19] (i.e., without vegetation compensation) and the one presented here, with the three different possible dipole orientation distributions. They are then converted into volumetric moisture m_v using the mixing model in [49],[2] considering that the soil in the Demmin area consists mostly of

[2]See footnote 1.

loamy sand, with percentages of sand and clay of 68% and 7%, respectively [44]. Two samples of obtained m_v maps, one without compensation and one with "uniform" vegetation compensation, are shown in Fig. 6(c) and (d), respectively. In this scenario, the inversion rates strongly vary from one acquisition to another: In particular, in the first acquisition (on April 19), they are 7% for no compensation, and 25%, 24%, and 17% for the "uniform," "vertical," and "horizontal" compensation cases, respectively; they remain substantially stable until mid May, then they start to progressively decrease, reaching very low values (0.1%, 2%, 1%, and 3% for the four cases) on July 12, and finally, they raise again in the last two acquisitions, so that in the August 2 acquisition, they are 29% for no compensation, and 40%, 25%, and 32% for the "uniform," "vertical" and "horizontal" compensation cases, respectively. With regard to the negative power problem, the situation is more stable: The percentage of points suffering from the negative power problem is about 6% in the April 19 acquisition, and then it moves to values around 20% in the other acquisitions. Finally, with regard to pixels for which double-bounce is dominant, they are about 30%, except for the mid and late May acquisitions, in which they raise to about 70%.

In order to explore the validity limits of the PTSTCM, and to better compare the proposed different kinds of vegetation corrections, we show the results for three different periods of the year. In the first period (April 19–May 16, 2006) the vegetation was mostly in an early stage of growth and its average height was low (ranging from nearly zero, for corn fields, to more than 1 m, for rape fields). In the second one (May 24–June 13, 2006) the various crop types were in an intermediate stage of growth, presenting significant average heights in many cases (ranging from 20–30 cm, for corn fields, to about 170 cm, for rape fields). Finally, in the last period (June 21–August 2, 2006) the vegetation was in an advanced stage of growth, with average heights larger than 1 m in most cases (ranging from about 80 cm, for wheat fields, to more than 2 m, for corn fields). We note that there are a couple of noticeable exceptions to these general trends: In particular, the vegetation cycle of sugar beet and corn cultivations (plantation in spring) is temporally shifted with respect to the other winter cultivations (plantation in autumn). Therefore, the fields relevant to these two crops are completely bare during the first period because plantation takes place in April. On the other hand, in the last couple of acquisition dates, winter barley and rape are already harvested, leaving almost bare-soil fields (this justifies the higher inversion rates in these acquisitions).

In Figs. 7–9 the results obtained for the three periods without vegetation compensation and with the three different kinds of compensation are reported: The quantitative measures of performance for each of the considered scatterplots are reported in Table I. We indicate with N the number of fields for which inversion is successful (i.e., for which, in at least 20% of the pixels, the modified correlation coefficient can be defined, and obtained values are inside the physically allowable range) for all of the acquisition dates of the considered period. The total number of fields considered in this paper is 13.

It can be seen that, as expected, none of the approaches performs well on the whole vegetation cycle. In particular, in the first period, when vegetation is mostly in an early stage of growth, the highest values of N are obtained. In this case, the best results are provided by the method based on dipoles with random uniformly distributed orientations, which seems to be a favorable model for early stage vegetation. This also justifies the choice made in Section IV-A of considering this kind of vegetation model. However, acceptable performances are obtained also by considering mainly horizontally oriented dipoles for the volume contribution.

In the second period, conversely, the best performance in terms of both ρ and rmse is provided by the method based on mainly vertically oriented dipoles: this can be related to a preferential vertical orientation of the plants' trunks when the growth cycle is not yet in an advanced stage. However, a very small ME is obtained for uniformly distributed orientations. Note also (see Fig. 8) that the best performances are obtained for corn fields (with all the models, and in particular for uniformly and vertically distributed orientations) and for sugar beet fields (with horizontally oriented dipoles), for which, as highlighted above, the growth cycle is temporally shifted with respect to the other cultivations, so that they are in an early stage of growth also in this second period.

Finally, in the third period, none of the methods provides reasonably accurate results, due to the presence of high and dense vegetation. Anyway, the best results are once again obtained considering mainly vertically oriented dipoles.

In summary, here, we have shown that, as expected, the PTSTCM can be used only for moderately vegetated areas and that, within this domain of applicability, the volumetric model employing uniformly distributed dipole orientations is preferable to the others in the majority of cases. Accordingly, we can conclude that, for moderate vegetation, when no precise information on the vegetation type is available, PTSTCM with uniform dipole orientation can be used. However, in order to provide more quantitative validity limits, a further analysis is still needed. This analysis is performed in the following, where validity limits in terms of vegetation height or in terms of the value of the cross-polarized ratio, are provided, and the PTSTCM is compared with 3CMs.

C. Comparison With 3CMs

Results presented earlier show that PTSTCM provides excellent [see Fig. 5(b)] or good [see Fig. 7(b) and (c)] estimates in the presence of a moderate vegetation, when a dominant surface scattering component is accompanied by a nonnegligible volume scattering component; conversely, it provides very poor [see Fig. 8(b)–(d)] or completely unreliable (see Fig. 9) results when vegetation density and height increase, so that surface scattering is not the main scattering mechanism, and in addition to volume scattering, a nonnegligible double-bounce scattering component is present. In order to deal with this latter situation, 3CMs are needed, which include also double-bounce scattering [11], and possibly, more refined, parametric/variable vegetation volumetric scattering models [21]–[23]. We expect that our PTSTCM, which considers a more refined surface scattering model, is preferable for low vegetation, whereas 3CM-based methods, which consider more refined

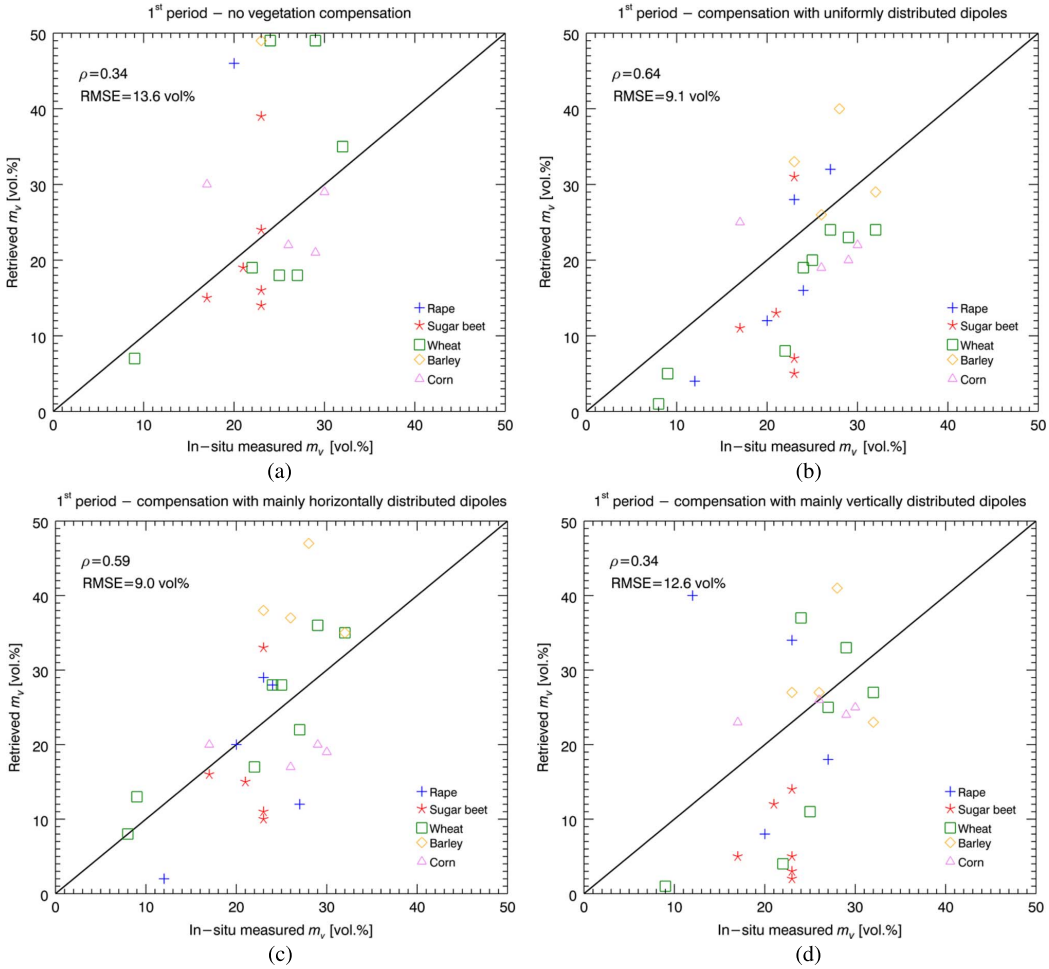

Fig. 7. Scatterplot of the retrieval results versus measured ground truth for the first period. (a) Without vegetation compensation. (b) With vegetation compensation modeled via dipoles with random uniformly distributed orientations. (c) With vegetation compensation modeled via mainly horizontally oriented dipoles. (d) With vegetation compensation modeled via mainly vertically oriented dipoles.

vegetation models, are preferable for high or very high vegetation. In order to check this expectation and to give a more quantitative meaning to the expressions "low vegetation" and "high or very high vegetation," we here compare results of PTSTCM and 3CM over two fields with different vegetation growth behaviors, namely fields labeled as 222 (corn field, see Fig. 10) and 230 (wheat field, see Fig. 11) in [44]. 3CM retrieval results are taken from [11]; in fact, in [11], the same AgriSAR data set introduced in Section IV-B is used, and data are presented in a format useful for our discussion. In the following, we also consider the same ground-truth data as in [11], and a data display format similar to that employed there. In Figs. 10(a) and 11(a), "no compensation" indicates the standard PTSM of [19], "uniform compensation" indicates PTSTCM with a uniform distribution for dipole orientation, and "horizontal compensation" and "vertical compensation" indicate PTSTCM with a prevalently horizontal and prevalently vertical distribution for dipole orientation, respectively. In Figs. 10(b) and 11(b), blue symbols indicate that soil moisture is estimated from the surface component of the 3CM, whereas red symbols indicate that retrieval is obtained from the double-bounce component of the 3CM. In addition, "Bragg" indicates the usual three-component Freeman decomposition, "X-Bragg" indicates that the X-Bragg model [10], with an *a priori* fixed value of the roughness parameter, is used for the surface component; and "volumes 1, 2, and 3" indicate three modifications of the dipole-cloud model for the volumetric component: volume 1 indicates the decomposition using a random oriented volume with particles of arbitrary shape, volume 2 indicates the decomposition using a weakly oriented volume of dipoles, and volume 3 indicates the decomposition using a strongly oriented volume of dipoles. Further details can be found in [11]. Note that AgriSAR data are also used in [22], [23] to analyze the more refined parametric volumetric model there presented; however, data presented in [22] and [23] are not in the format useful for the comparison here. In addition, acquisitions of May 2006 are not considered in [22], [23]. In spite of that, since different methods considered in [11] cover a wide range of shape and orientation parameter values, we believe that a reasonable estimate of the results of the parametric volume model method used in [22] and [23] can be obtained by considering, for each acquisition, the best retrieval result among those of all the methods considered in [11].

Let us first consider the corn field 222. Comparison of Fig. 10(a) and (b) shows that up to the last acquisition of June (day 172), corresponding to vegetation height smaller than about 50 cm, PTSTCM provides better results than 3CMs,

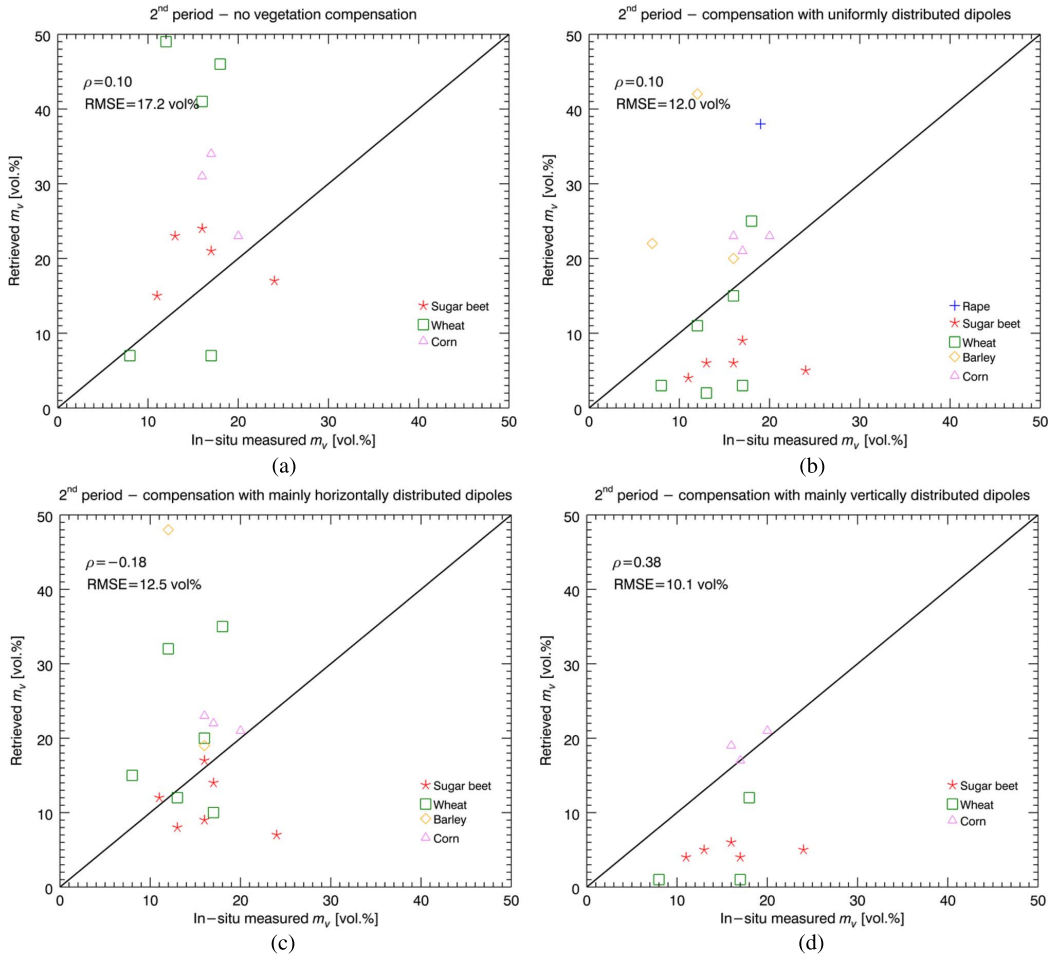

Fig. 8. Scatterplot of the retrieval results versus measured ground truth for the second period. (a) Without vegetation compensation. (b) With vegetation compensation modeled via dipoles with random uniformly distributed orientations. (c) With vegetation compensation modeled via mainly horizontally oriented dipoles. (d) With vegetation compensation modeled via mainly vertically oriented dipoles.

and relative error is always smaller than 30% (and in most cases, smaller than 20%). In addition, all the three considered dipole orientation distributions provide similar results, which are better than results obtained by PTSM (i.e., without compensation of vegetation).[3] This is coherent with the fact that, in this case, surface scattering is dominant with respect to a nonnegligible volume scattering component, so that using a more refined surface model and a simple volume model is more appropriate than using a more refined volume model and a simple surface model. Conversely, for the acquisitions of July and August, corresponding to vegetation higher than about 1 m, the best results are obtained by 3CMs; in particular, in the last two acquisitions, results obtained from the double-bounce component are better than those obtained from the surface scattering component. This shows the importance of including double bounce for such a high vegetation.

Let us now move to consider the wheat field 230. Comparison of Fig. 11(a) and (b) shows that, for the first three acquisitions (April and first part of May, up to day 130), again corresponding to vegetation height smaller than about 50 cm, PTSTCM provides better results than 3CMs; in particular, in the first two acquisitions, the relative error for PTSTCM with uniformly and vertically oriented dipole models is always not larger than about 20%, whereas in the third acquisition, the PTSTCM relative error is a bit larger than 30%, but no useful result is obtained by the 3CM. Again, this is coherent with the fact that, in this case, surface scattering is dominant with respect to a nonnegligible volume scattering component, similarly to what explained for field 222. Conversely, for the two subsequent May acquisitions (around day 140), no valid retrieval results are obtained by our PTSTCM. However, it must be noted that the same holds for 3CMs if retrieval is obtained from the surface scattering component and only retrievals based on the double-bounce component are successful. In fact, for these acquisitions, the real part of the HH-VV correlation turns out to be negative; this indicates a dominance of the double-bounce component. This is most likely related to the vegetation shape and density at this intermediate growth stage. Starting from the June acquisitions, corresponding to vegetation higher than about 50 cm, the best results are obtained by the 3CMs. However, for the June acquisitions, PTSTCM with uniform dipole orientation distribution provides reasonable results. This is not the case for July and August acquisitions, corresponding

[3]This is with the exception of the first two acquisitions, for which the field was bare soil, so that also the uncompensated method provides accurate results.

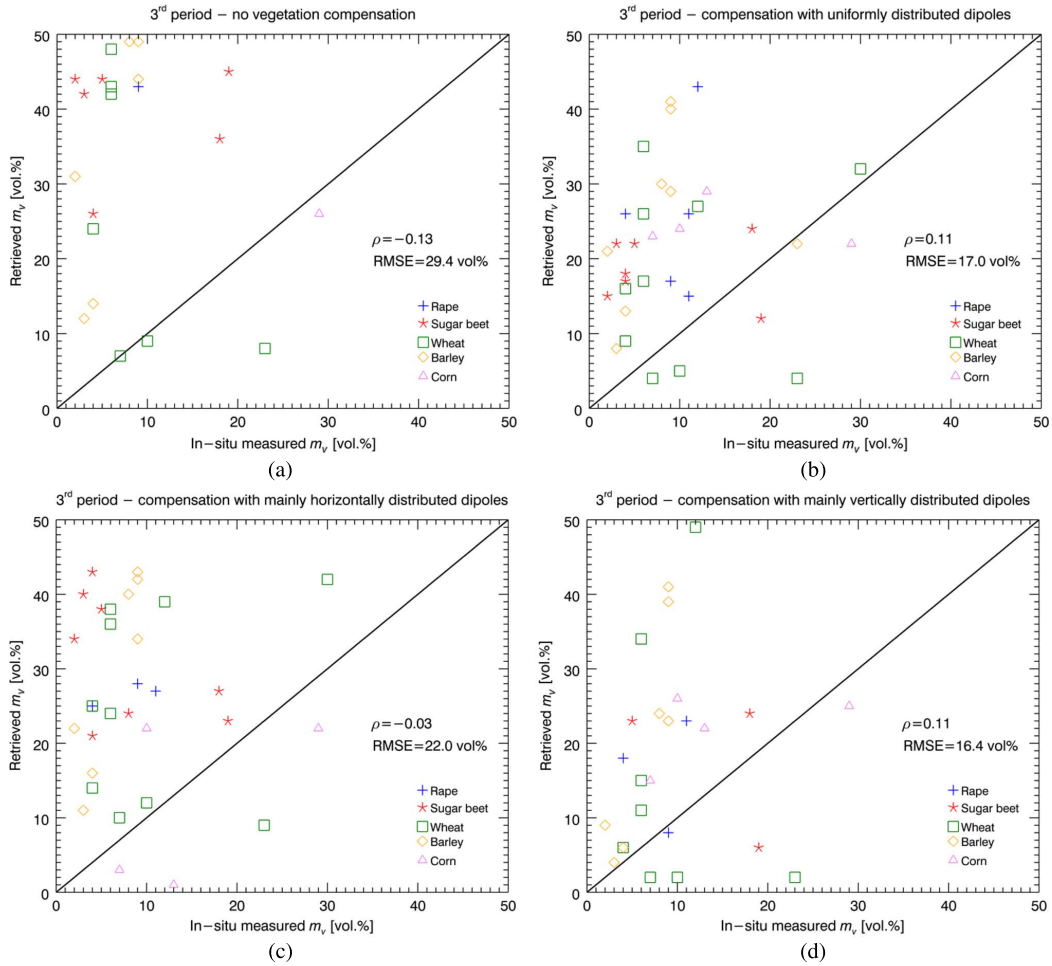

Fig. 9. Scatterplot of the retrieval results versus measured ground truth for the third period. (a) Without vegetation compensation. (b) With vegetation compensation modeled via dipoles with random uniformly distributed orientations. (c) With vegetation compensation modeled via mainly horizontally oriented dipoles. (d) With vegetation compensation modeled via mainly vertically oriented dipoles.

TABLE I
PERFORMANCES OF THE VOLUMETRIC SOIL MOISTURE RETRIEVAL APPROACHES

	I PERIOD (APRIL 19-MAY 16, 2006) EARLY STAGE OF GROWTH				II PERIOD (MAY 24-JUNE 13, 2006) INTERMEDIATE STAGE OF GROWTH				III PERIOD (JUNE 21-AUGUST 2, 2006) ADVANCED STAGE OF GROWTH			
	ME [vol. %]	RMSE [vol. %]	ρ	N	ME [vol. %]	RMSE [vol. %]	ρ	N	ME [vol. %]	RMSE [vol. %]	ρ	N
No compensation	4.0	13.6	0.34	9	10.0	17.2	0.10	6	24.0	29.4	−0.13	8
"Uniform dipoles" compensation	−4.4	9.1	0.64	12	−0.2	12.0	0.10	9	12.0	17.0	0.11	10
"Horizontal dipoles" compensation	−0.6	9.0	0.59	12	3.6	12.5	−0.18	8	17.0	22.0	−0.03	10
"Vertical dipoles" compensation	−3.8	12.6	0.34	12	−7.4	10.1	0.38	5	8.6	16.4	0.11	9

to a vegetation height of about 80 cm. For these latter acquisitions, the 3CM results are by far better than the PTSTCM ones.

These results suggest that PTSTCM is preferable up to a vegetation height of about 50 cm, whereas 3CM-based methods are preferable for vegetation height of about 80 cm or higher. In intermediate situations (i.e., vegetation height between 50 and 80 cm) results of the two approaches are usually similar, with a slight preference for 3CMs.

In the analysis performed earlier, we have attributed the decreasing accuracy of PTSTCM with time to the increasing vegetation height. It must be also noted that soil moisture decreases with time, so that one could infer that PTSTCM

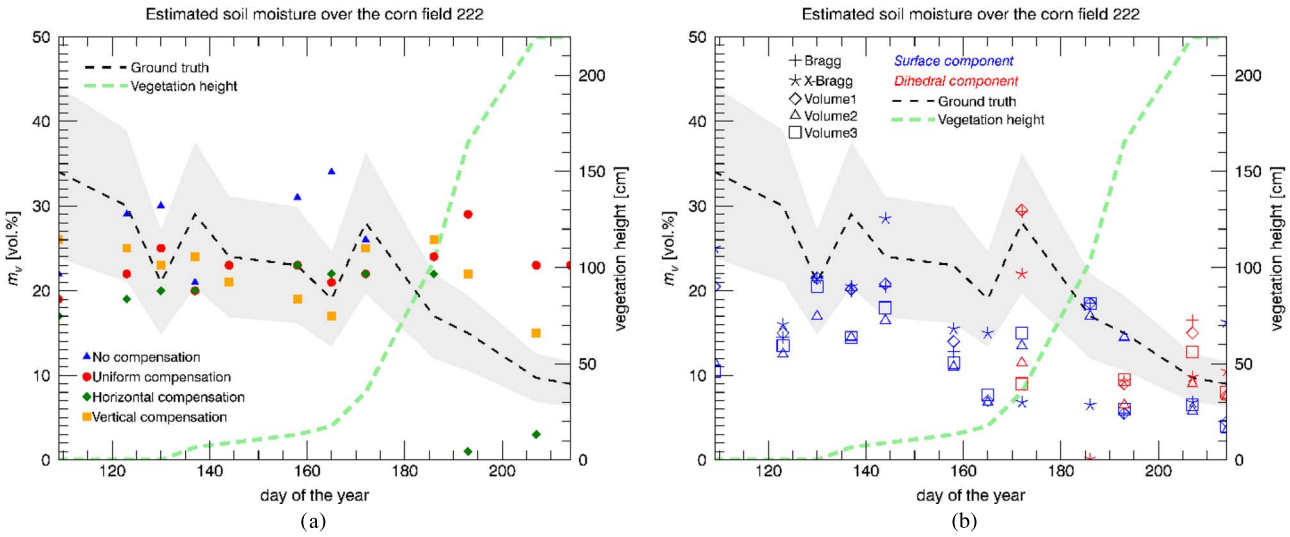

Fig. 10. Estimated average soil moisture over the corn field 222 inverted via (a) the proposed method and (b) the 3CM method of [11]. The *in situ* estimated soil moisture (as taken from [11]) is indicated by the black dashed line, and the ±30% variation region is highlighted in gray.

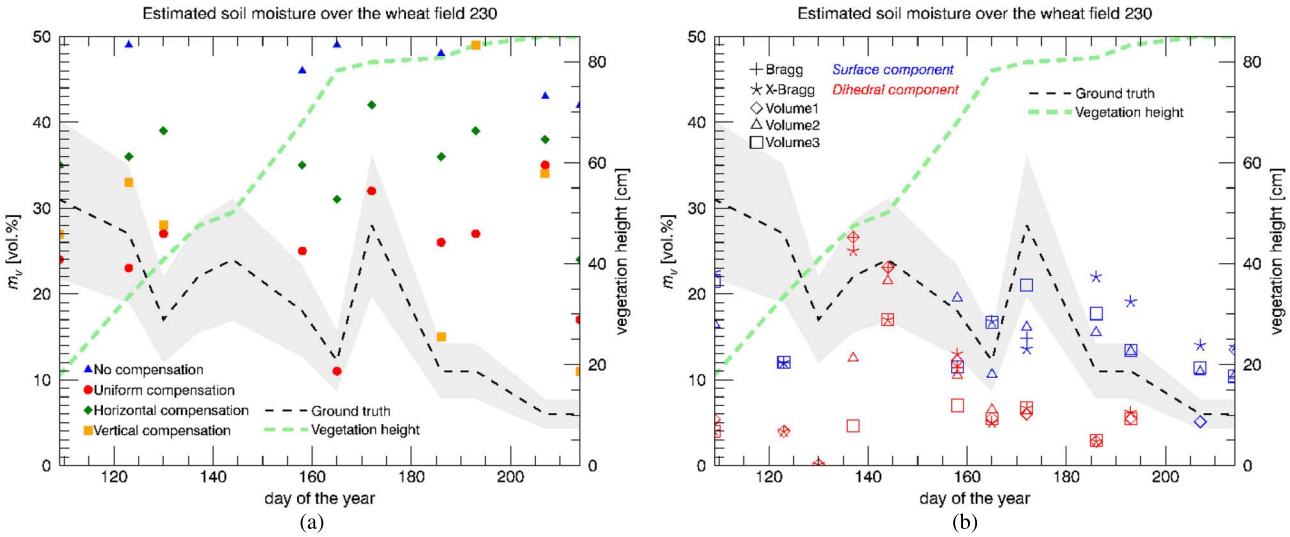

Fig. 11. Estimated average soil moisture over the wheat field 230 inverted via (a) the proposed method and (b) the 3CM method of [11]. The *in situ* estimated soil moisture (as taken from [11]) is indicated by the black dashed line and the ±30% variation region is highlighted in gray.

decreasing accuracy may be also due to a reduced sensitivity of the method for low values of the soil moisture. However, this is excluded by the sensitivity analysis performed in Section III-C, so that we can confirm that the decisive factor is the increasing vegetation height.

In order to further support the conclusions above, in Fig. 12, we plot the modulus of the soil moisture relative error versus vegetation height for fields 222 and 230, by considering PTSTCM with uniformly distributed dipoles (triangular symbols) and the best, for each acquisition, among the 3CMs of [11] (asterisk symbols). This simulates a situation in which no information on the vegetation type is available, and the variable vegetation model of [22], [23] is used for 3CM. The plots of Fig. 12 show that, for a vegetation height smaller than 50 cm, PTSTCM results are more accurate than 3CM ones (with only one exception), and in half of the cases, this improvement is greater than 20%. The average modulus of the relative error (in short, the average relative error) is 18.5% for PTSTCM and 34% for 3CM. For vegetation height between 50 and 80 cm, there is no clear advantage of one method with respect to the other (but, on the average, the relative error is smaller for 3CM, i.e., 14.3%, against a 20.3% for PTSTCM), whereas for larger vegetation height, very small errors are obtained by 3CM. Moreover, PTSTCM relative error is always larger than 50% (and often even larger than 100%). In this final case, the average relative error is 18.7% for 3CM and 134% for PTSTCM.

Finally, it is useful to analyze the behavior of PTSTCM and 3CM as a function of some parameter that can be computed directly from SAR data. Results of Section III-B, and in particular condition (20), suggest that such a parameter can be the value of the cross-polarized ratio. Accordingly, in Fig. 13, we plot the modulus of the soil moisture relative error versus cross-polarized ratio for fields 222 and 230, by considering PTSTCM with uniformly distributed dipoles (triangular symbols) and the best, for each acquisition, among the 3CMs of [11] (asterisk symbols). It turns out that for a cross-polarized ratio

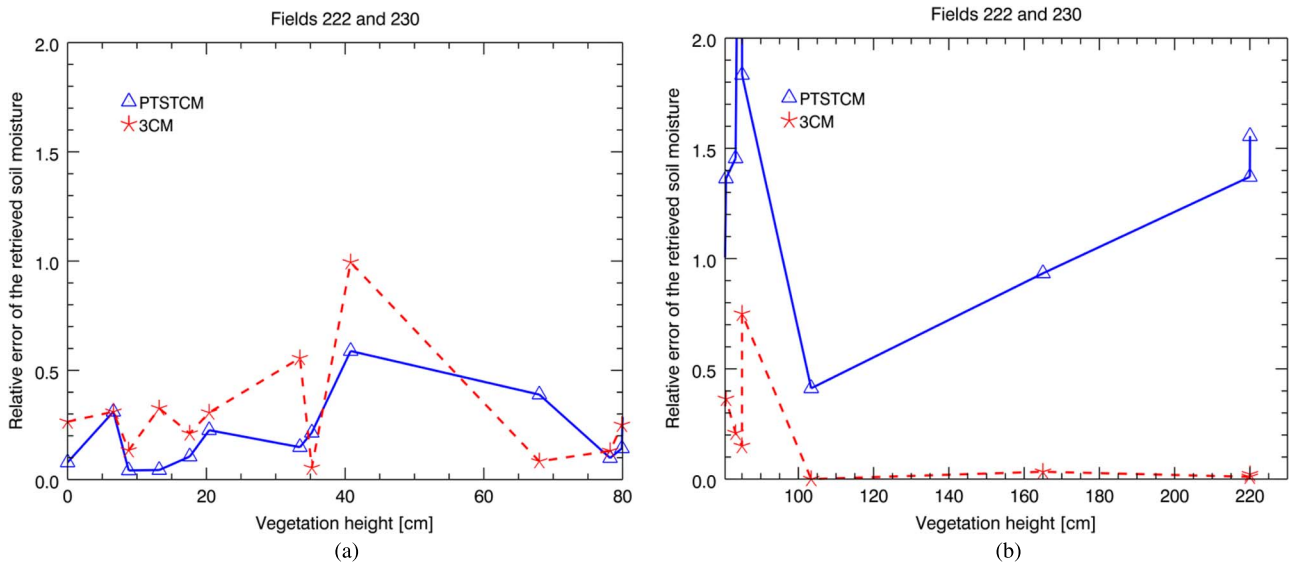

Fig. 12. Absolute value of soil moisture relative error versus vegetation height, fields 222 and 230, for PTSTCM (triangles) and 3CM (asterisks). (a) Vegetation height smaller than 80 cm and (b) larger than 80 cm.

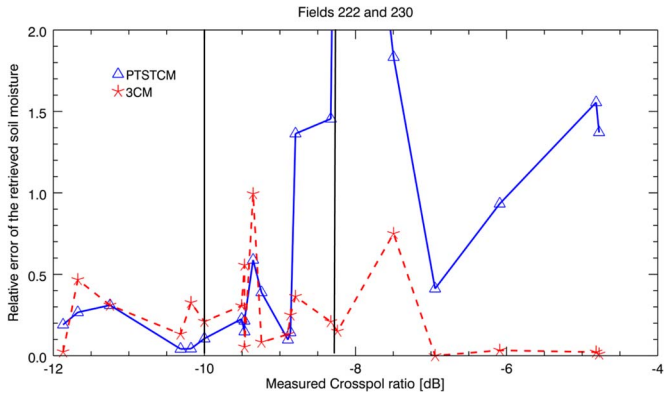

Fig. 13. Absolute value of soil moisture relative error versus cross-polarized ratio, fields 222 and 230, for PTSTCM (triangles) and 3CM (asterisks).

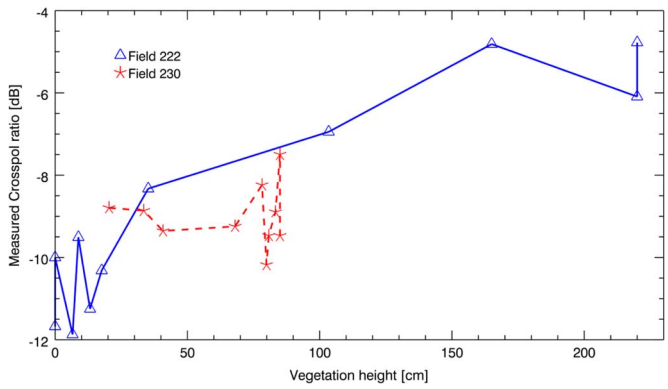

Fig. 14. Cross-polarized ratio versus vegetation height, for fields 222 (triangles) and 230 (asterisks).

smaller than 0.1 (i.e., smaller than −10 dB) PTSTCM results are more accurate than those of 3CM (the average relative error is 14.5% for PTSTCM and 24.3% for 3CM); for a cross-polarized ratio in the range of 0.1–0.15 (i.e., from −10 to −8.25 dB), there is no clear advantage of one method with respect to the other (the average relative error is 33.9% for 3CM and 37.5% for PTSTCM), and for cross-polarized ratio with values greater than 0.15 (i.e., greater than −8.25 dB), very small errors are obtained by 3CM, whereas PTSTCM relative error is always larger than 40% (and often even larger than 100%). In this final case, the average relative error is 15.3% for 3CM and 118% for PTSTCM.

It is worth noting at this point that, although the behavior of soil moisture retrieval as a function of vegetation height is similar to its behavior as a function of the cross-polarized ratio, this last parameter cannot be in general used as a measure of vegetation height: In fact, the plot of Fig. 14 shows that, while for field 222 a clear increasing trend of crosspol with respect to vegetation height can be noted, this is not the case for field 230. Finally, it must also be mentioned that, in [11], the rape field labeled as 101 is considered. For this field, the vegetation height was lower than 50 cm only for the first acquisition, and for all the acquisitions (including the first), the crosspol ratio is higher than 0.2, indicating that our model cannot be employed there. In fact, it turns out that, for this field, parametric 3CM always provides better results than PTSTCM. This further confirms the conclusion of our analysis.

In summary, here, we have shown that for vegetation height smaller than 50 cm or cross-polarized ratio smaller than 0.1, PTSTCM provides better results with respect to existing parametric 3CMs. For vegetation height ranging from 50 to 80 cm or cross-polarized ratio ranging from 0.1 to 0.15, there is no clear advantage of using one method or the other. For vegetation height larger than 80 cm or cross-polarized ratio larger than 0.15, parametric 3CMs provide much better results than PTSTCM. It is here also useful to recall that, as stated in Section III-B, PTSTCM cannot be used if the real part of the vegetation-corrected HH-VV correlation is negative. Finally, we note that applicability of the methods may be related not only to vegetation height but also to other vegetation indexes

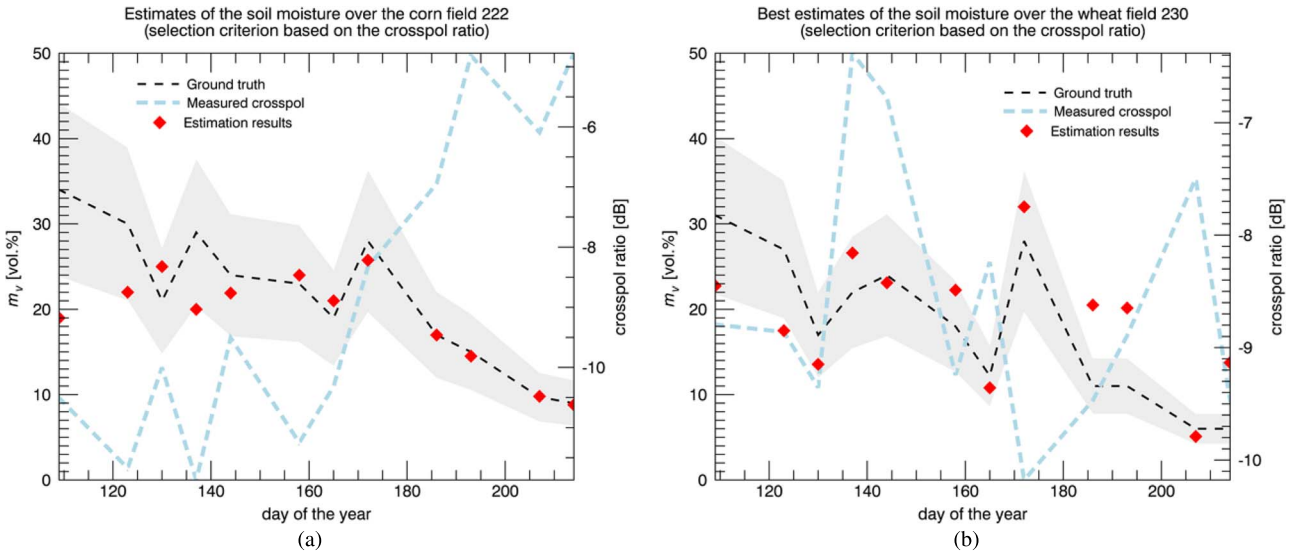

Fig. 15. Retrieval results obtained by using the PTSTCM and 3CM combined method. The selection criterion is based on the cross-polarized ratio and signum of the real part of copolarized correlation. (a) Field 222 and (b) Field 230.

such as the Leaf Area Index (LAI). However, it is much easier to *in situ* measure vegetation height than LAI, so that it is much more likely that vegetation height is known than LAI. That is why here we have preferred to focus our analysis on vegetation height.

D. Combined Use of PTSTCM and 3CM

Here, we propose a way to combine the PTSTCM with 3CM of [22], [23]. In fact, results of the earlier analysis and of Section III-B, suggest that simple criteria can be used for the selection between the use of PTSTCM with uniformly distributed dipoles and 3CM of [22] and [23] on a pixel-by-pixel basis, so that a more general method is obtained.

The choice criterion can be based on the value of the cross-polarized ratio and on the signum of the real part of the HH-VV correlation. In particular, if the cross-polarized ratio is smaller than 0.1 and the real part of the HH-VV correlation is positive, then the PTSTCM must be used first: If retrieval is successful, the obtained value is the desired output; otherwise, 3CM must be used. If the cross-polarized ratio is larger than or equal to 0.1 and smaller than 0.15, and the real part of the HH-VV correlation is positive, then both methods must be used: If both are successful, then the output is computed as the average of the two retrieved values; otherwise, the output is the retrieved value of the successful method, if any. Finally, if the cross-polarized ratio is larger than or equal to 0.15 or the real part of the HH-VV correlation is negative, then the 3CM must be used first: If retrieval is successful, the obtained value is the desired output; otherwise, PTSTCM must be used. The retrieval results obtained by applying this criterion to fields 222 and 230 are shown in Fig. 15. For the field 222, a significant overall improvement with respect to the graphs of Fig. 10 is obtained, and the relative error is in most cases well below 10%. Moreover, for the field 230, a significant improvement with respect to the graphs of Fig. 11 is obtained, but rather, large errors are still obtained in some of the late acquisitions.

In conclusion, combined use of PTSTCM and 3CM according to the proposed criterion allows us to significantly improve soil moisture results with respect to the cases in which PTSTCM and 3CM are individually employed.

V. Conclusion

In this paper, we have inserted the PTSM, presented in [13], into a two-component scattering model, thus obtaining a polarimetric two-scale two-component model (PTSTCM). In particular, we use the PTSM to describe the surface scattering component, and a randomly (uniformly, vertically, or horizontally) oriented thin dipole model to describe the volume scattering contribution from the vegetation layer that covers the scattering surface. We have shown that suitable combinations of the NRCS and HH-VV correlation, which we term "modified copolarized ratio" and "modified copolarized correlation coefficient," are related only to the surface parameters because, in principle (i.e., if the employed volumetric model is sufficiently accurate in the considered case), the dependence on the unknown volumetric contribution intensity cancels out. Therefore, they can be used for soil moisture retrieval under moderate vegetation cover. The behavior of the method with respect to the negative power problem has been discussed, showing that this problem is significantly mitigated, and a theoretical analysis of the sensitivity of retrieval results with respect to the different possible error sources has been also performed.

We have then tested the PTSTCM-based retrieval method by applying it to polarimetric SAR data acquired on areas for which, at the same time of SAR acquisitions, ground measurements of soil moisture were performed. To this end, both SMEX'03 and AGRISAR'06 data have been used. In addition, results of PTSTCM have been compared with those of available 3CMs employing more simplified surface scattering models but more refined volumetric ones [22], [23]. It has turned out that the use of PTSTCM is more convenient for low vegetation (vegetation height lower than about 50 cm) because

surface scattering is better modeled. The results of PTSTCM and 3CMs are also similar, with a slight preference for 3CMs, for intermediate vegetation (vegetation height between about 50 and about 80 cm), because the surface component is still important, but its significance decreases and double bounce (ignored by PTSTCM) starts playing a role. Finally, 3CMs are more convenient for high vegetation (vegetation height greater than about 80 cm) because the advantage of the more refined surface scattering model of PTSTCM is of little importance in this case, whereas it is necessary to account for double-bounce scattering. The convenience of using PTSTCM has turned out to be also related to the values of measured cross-polarized ratio and copolarized correlation: in fact, PTSTCM is preferable when cross-polarized ratio is not larger than 0.1, and at the same time, the real part of the copolarized correlation is positive. In all other cases, 3CMs are preferable, and they often provide accurate results even in the case of dihedral dominance.

Finally, as a conclusion of the performed analysis, we have suggested a method in which, pixel by pixel, based on the values of the cross-polarized ratio and on the signum of the real part of the copolarized correlation, either the PTSTCM or a three-component decomposition with variable vegetation volume model is employed to retrieve soil moisture. We have shown that this combination of methods provides very good soil moisture results on the entire vegetation cycle.

At this point, it is useful to note that the only situation in which combination of the proposed PTSTCM with 3CM is not appropriate is the case of dominant surface scattering and a secondary nonnegligible dihedral component. Improvement of our method to properly account for this case goes beyond the scope of this paper and is matter of our future work.

Finally, we must remark that conclusions reported here refer to the case of flat topography, due to the characteristics of considered test sites. The proposed technique, with proper modifications to the surface model [14], may also be applied to hilly or mountainous sites, provided that site topography is known; however, assessing the method performance in these cases still requires further future work.

APPENDIX

Here, we show how (1)–(6) can be obtained from [19, Eq. (8)], which we report here for the sake of completeness:

$$\begin{cases} \left\langle |S_{vv}|^2 \right\rangle_{|\zeta,a,b} = C_{0,0}^{vv} + \left(C_{2,0}^{vv} + C_{0,2}^{vv} + 2\frac{\mathrm{Re}\left\{C_{0,0}^{hv}\right\} - C_{0,0}^{vv}}{\sin^2\vartheta} \right) \sigma^2 \\ \left\langle |S_{hh}|^2 \right\rangle_{|\zeta,a,b} = C_{0,0}^{hh} + \left(C_{2,0}^{hh} + C_{0,2}^{hh} + 2\frac{\mathrm{Re}\left\{C_{0,0}^{hv}\right\} - C_{0,0}^{hh}}{\sin^2\vartheta} \right) \sigma^2 \\ \left\langle S_{hh} S_{vv}^* \right\rangle_{|\zeta,a,b} = C_{0,0}^{hv} + \left(C_{2,0}^{hv} + C_{0,2}^{hv} + \frac{C_{0,0}^{hh} + C_{0,0}^{vv} - 2C_{0,0}^{hv}}{\sin^2\vartheta} \right) \sigma^2 \\ \left\langle |S_{hv}|^2 \right\rangle_{|\zeta,a,b} = \left(C_{0,0}^{hh} + C_{0,0}^{vv} - 2\mathrm{Re}\left\{C_{0,0}^{hv}\right\} \right) \frac{\sigma^2}{\sin^2\vartheta} \end{cases} \tag{27}$$

where

$$C_{k,n-k}^{pq} = \frac{1}{n!}\binom{n}{k} \frac{\partial^n \left(s_0^2 W_n k^4 \cos^4\vartheta_l F_p F_q^* \right)}{\partial a^k \partial b^{n-k}} \bigg|_{a=b=0}. \tag{28}$$

Accordingly

$$\begin{aligned} C_{0,0}^{pq} &= s_0^2\, W_n (2k\sin\vartheta_l)(k\cos\vartheta_l)^4 F_p(\vartheta_l) F_q^*(\vartheta_l)\big|_{a=b=0} \\ &= s_0^2 W_n (2k\sin\vartheta)(k\cos\vartheta)^4 F_p(\vartheta) F_q^*(\vartheta) \end{aligned} \tag{29}$$

so that

$$C_{0,0}^{vv} = s_0^2 f_s,\ C_{0,0}^{hh} = s_0^2 f_s |\beta_r|^2,\ C_{0,0}^{hv} = s_0^2 f_s \beta_r \tag{30}$$

$$C_{2,0}^{pq} + C_{0,2}^{pq} = s_0^2 C_2^{pq}. \tag{31}$$

Let us now consider the first equation of (27):

$$\begin{aligned} &\left\langle |S_{vv}|^2 \right\rangle_{|\zeta,a,b} \\ &= C_{0,0}^{vv} + \left(C_{2,0}^{vv} + C_{0,2}^{vv} + 2\frac{\mathrm{Re}\left\{C_{0,0}^{hv}\right\} - C_{0,0}^{vv}}{\sin^2\vartheta} \right) \sigma^2 \\ &= C_{0,0}^{vv} \left[1 + \left(\frac{C_{2,0}^{vv} + C_{0,2}^{vv}}{C_{0,0}^{vv}} + 2\frac{\mathrm{Re}\left\{C_{0,0}^{hv}\right\} - C_{0,0}^{vv}}{C_{0,0}^{vv}\sin^2\vartheta} \right) \sigma^2 \right] \\ &= s_0^2 f_s \left[1 + \left(\frac{C_2^{VV}}{f_s} + 2\frac{\mathrm{Re}\{\beta_r\} - 1}{\sin^2\vartheta} \right) \sigma^2 \right] \\ &= s_0^2 f_s \left[1 - \left(2\mathrm{Re}\left\{ \frac{1-\beta_r}{\sin^2\vartheta} \right\} - \frac{C_2^{VV}}{f_s} \right) \sigma^2 \right] \end{aligned} \tag{32}$$

which is the first equation of (1). Similarly

$$\begin{aligned} &\left\langle |S_{hh}|^2 \right\rangle_{|\zeta,a,b} \\ &= C_{0,0}^{hh} + \left(C_{2,0}^{hh} + C_{0,2}^{hh} + 2\frac{\mathrm{Re}\left\{C_{0,0}^{hv}\right\} - C_{0,0}^{hh}}{\sin^2\vartheta} \right) \sigma^2 \\ &= C_{0,0}^{hh} \left[1 + \left(\frac{C_{2,0}^{hh} + C_{0,2}^{hh}}{C_{0,0}^{hh}} + 2\frac{\mathrm{Re}\left\{C_{0,0}^{hv}\right\} - C_{0,0}^{hh}}{C_{0,0}^{hh}\sin^2\vartheta} \right) \sigma^2 \right] \\ &= s_0^2 f_s |\beta_r|^2 \left[1 + \left(\frac{C_2^{HH}}{f_s|\beta_r|^2} + 2\frac{\mathrm{Re}\left\{\frac{1}{\beta_r^*}\right\} - 1}{\sin^2\vartheta} \right) \sigma^2 \right] \\ &= s_0^2 f_s |\beta_r|^2 \left[1 + \left(2\mathrm{Re}\left\{ \frac{1-\beta_r}{\beta_r \sin^2\vartheta} \right\} + \frac{C_2^{HH}}{f_s|\beta_r|^2} \right) \sigma^2 \right] \end{aligned} \tag{33}$$

which is the second equation of (1), and

$$\begin{aligned} &\left\langle S_{hh} S_{vv}^* \right\rangle_{|\zeta,a,b} \\ &= C_{0,0}^{hv} + \left(C_{2,0}^{hv} + C_{0,2}^{hv} + \frac{C_{0,0}^{hh} + C_{0,0}^{vv} - 2C_{0,0}^{hv}}{\sin^2\vartheta} \right) \sigma^2 \\ &= C_{0,0}^{hv} \left[1 + \left(\frac{C_{2,0}^{hv} + C_{0,2}^{hv}}{C_{0,0}^{hv}} + \frac{C_{0,0}^{hh} + C_{0,0}^{vv} - 2C_{0,0}^{hv}}{C_{0,0}^{hv}\sin^2\vartheta} \right) \sigma^2 \right] \\ &= s_0^2 f_s \beta_r \left[1 + \left(\frac{C_2^{HV}}{f_s\beta_r} + \frac{\beta_r^* + \frac{1}{\beta_r} - 2}{\sin^2\vartheta} \right) \sigma^2 \right] \\ &= s_0^2 f_s \beta \left[1 + \left(\frac{\beta_r^* - 1 + \frac{1}{\beta_r} - 1}{\sin^2\vartheta} + \frac{C_2^{HV}}{f_s\beta_r} \right) \sigma^2 \right] \\ &= s_0^2 f_s \beta_r \left[1 + \left(\frac{1-\beta_r}{\beta_r \sin^2\vartheta} - \frac{1-\beta_r^*}{\sin^2\vartheta} + \frac{C_2^{HV}}{f_s\beta_r} \right) \sigma^2 \right] \end{aligned} \tag{34}$$

which is the third equation of (1). Finally

$$\begin{aligned}\left\langle |S_{hv}|^2 \right\rangle_{|\zeta,a,b} &= \left(C_{0,0}^{hh} + C_{0,0}^{vv} - 2\mathrm{Re}\left\{C_{0,0}^{hv}\right\}\right)\frac{\sigma^2}{\sin^2\vartheta} \\ &= C_{0,0}^{vv}\left(\frac{C_{0,0}^{hh} + C_{0,0}^{vv} - 2\mathrm{Re}\left\{C_{0,0}^{hv}\right\}}{C_{0,0}^{vv}}\right)\frac{\sigma^2}{\sin^2\vartheta} \\ &= s_0^2 f_s \frac{|\beta_r|^2 + 1 - 2\mathrm{Re}\left\{\beta_r\right\}}{\sin^2\vartheta}\sigma^2 \\ &= s_0^2 f_s \frac{|1-\beta_r|^2}{\sin^2\vartheta}\sigma^2 \end{aligned} \tag{35}$$

which is the last equation of (1).

ACKNOWLEDGMENT

The authors wish to thank the anonymous reviewers for their very detailed comments that helped improve the quality of the paper and the European Space Agency for the AGRISAR data obtained through the EO Project id14445 titled "Soil Moisture Retrieval via SAR data, based on a Polarimetric Two-Scale-Two-Component Model."

REFERENCES

[1] K. C. Kornelsen and P. Coulibaly, "Advances in soil moisture retrieval from synthetic aperture radar and hydrological applications," *J. Hydrol.*, vol. 476, pp. 460–489, Jan. 2013.

[2] F. T. Ulaby, K. Sarabandi, K. McDonald, M. Whitt, and M. C. Dobson, "Michigan microwave canopy scattering model," *Int. J. Remote Sens.*, vol. 11, no. 7, pp. 1223–1253, Jul. 1990.

[3] S.-K. Kweon and Y. Oh, "A modified water-cloud model with leaf angle parameters for microwave backscattering from agricultural fields," *IEEE Trans. Geosci. Remote Sens.*, vol. 53, no. 5, pp. 2802–2809, May 2015.

[4] S. Park, S.-K. Kweon, and Y. Oh, "Validity regions of soil moisture retrieval on the LAI-θ plane for agricultural fields at L-, C-, and X-Bands," *IEEE Geosci. Remote Sens. Lett.*, vol. 12, no. 6, pp. 1195–1198, Jun. 2015.

[5] L. Tsang and J. Kong, *Scattering of Electromagnetic Waves, Advanced Topics*, vol. 3. Hoboken, NJ, USA: Wiley, 2001.

[6] Y. Oh, K. Sarabandi, and F. T. Ulaby, "An empirical model and an inversion technique for radar scattering from bare soil surfaces," *IEEE Trans. Geosci. Remote Sens.*, vol. 30, no. 2, pp. 370–381, Mar. 1992.

[7] P. C. Dubois, J. J. van Zyl, and T. Engman, "Measuring soil moisture with imaging radars," *IEEE Trans. Geosci. Remote Sens.*, vol. 33, no. 4, pp. 915–926, Jul. 1995.

[8] J. Shi, J. Wang, A. Y. Hsu, P. E. O'Neill, and E. Engman, "Estimation of bare surface soil moisture and surface roughness parameter using L-band SAR image data," *IEEE Trans. Geosci. Remote Sens.*, vol. 35, no. 5, pp. 1254–1266, Sep. 1997.

[9] S. Le Hégarat-Mascle, M. Zribi, F. Alem, A. Weisse, and C. Loumagne, "Soil moisture estimation from ERS/SAR data: Toward an operational methodology," *IEEE Trans. Geosci. Remote Sens.*, vol. 40, no. 12, pp. 2647–2658, Dec. 2002.

[10] I. Hajnsek, E. Pottier, and S. R. Cloude, "Inversion of surface parameters from polarimetric SAR," *IEEE Trans. Geosci. Remote Sens.*, vol. 41, no. 4, pp. 727–744, Apr. 2003.

[11] I. Hajnsek, T. Jagdhuber, H. Schön, and K. P. Papathanassiou, "Potential of estimating soil moisture under vegetation cover by means of PolSAR," *IEEE Trans. Geosci. Remote Sens.*, vol. 47, no. 2, pp. 442–454, Feb. 2009.

[12] A. Merzouki, H. McNairn, and A. Pacheco, "Mapping soil moisture using RADARSAT-2 data and local autocorrelation statistics," *IEEE J. Sel. Topics Appl. Earth Observ. Remote Sens.*, vol. 4, no. 1, pp. 128–137, Mar. 2011.

[13] A. Iodice, A. Natale, and D. Riccio, "Retrieval of soil surface parameters via a polarimetric two-scale model," *IEEE Trans. Geosci. Remote Sens.*, vol. 49, no. 7, pp. 2531–2547, Jul. 2011.

[14] A. Iodice, A. Natale, and D. Riccio, "Retrieval of soil surface parameters via a polarimetric two-scale model in hilly or mountainous areas," in *Proc. SPIE SAR Image Anal., Modeling, Tech.*, Prague, Czech Republic, 2011, vol. 8179, pp. 1–9.

[15] X. Shen *et al.*, "Orientation angle calibration for bare soil moisture estimation using fully polarimetric SAR data," *IEEE Trans. Geosci. Remote Sens.*, vol. 49, no. 12, pp. 4987–4996, Dec. 2011.

[16] A. Natale, *Electromagnetic Models for the Retrieval of Surface Parameters Through SAR Data*, Ph.D. dissertation, Ingegneria Biomed., Elettronica Comun., Univ. Studi Napoli "Federico II," Napoli, Italy, Jan. 2012.

[17] M. Koch, T. Schmid, M. Reyes, and J. Gumuzzio, "Evaluating full polarimetric C- and L-band data for mapping wetland conditions in a semi-arid environment in central spain," *IEEE J. Sel. Topics Appl. Earth Observ. Remote Sens.*, vol. 5, no. 3, pp. 1033–1044, Jun. 2012.

[18] T. Jagdhuber, "Soil parameter retrieval under vegetation cover using SAR polarimetry," Ph.D. dissertation, Faculty Math. Nat. Sci., Univ. Potsdam, Potsdam, Germany, 2012.

[19] A. Iodice, A. Natale, and D. Riccio, "Polarimetric two-scale model for soil moisture retrieval via dual-pol HH-VV SAR data," *IEEE J. Sel. Topics Appl. Earth Observ. Remote Sens.*, vol. 6, no. 3, pp. 1163–1171, Jun. 2013.

[20] T. Jagdhuber, I. Hajnsek, A. Bronstert, and K. P. Papathanassiou, "Soil moisture estimation under low vegetation cover using a multi-angular polarimetric decomposition," *IEEE Trans. Geosci. Remote Sens.*, vol. 51, no. 4, pp. 2201–2215, Apr. 2013.

[21] D. Ballester-Berman, T. Jagdhuber, J.-M. Lopez-Sanchez, and F. Vicente-Guijalba, "Soil moisture estimation in vineyards by means of C-band radar measurements," in *Proc. EUSAR*, Berlin, Germany, Jun. 3–5, 2014, pp. 1–4.

[22] T. Jagdhuber, I. Hajnsek, and K. P. Papathanassiou, "Refined soil moisture estimation by means of L-band polarimetry," in *Proc. IEEE Int. Geosci. Remote Sens. Symp.*, Melbourne, Vic., Australia, Jul. 21–26, 2013, pp. 2325–2328.

[23] T. Jagdhuber, I. Hajnsek, and K. P. Papathanassiou, "An iterative generalized hybrid decomposition for soil moisture retrieval under vegetation cover using fully polarimetric SAR," *IEEE J. Sel. Topics Appl. Earth Observ. Remote Sens.*, vol. 8, no. 8, pp. 3911–3922, Aug. 2015.

[24] S. R. Cloude and E. Pottier, "A review of target decomposition theorems in radar polarimetry," *IEEE Trans. Geosci. Remote Sens.*, vol. 34, no. 2, pp. 498–518, Mar. 1996.

[25] N. Besic, G. Vasile, J. Chanussot, and S. Stankovic, "Polarimetric incoherent target decomposition by means of independent component analysis," *IEEE Trans. Geosci. Remote Sens.*, vol. 53, no. 3, pp. 1236–1247, Mar. 2015.

[26] A. Freeman and S. L. Durden, "A three-component scattering model for polarimetric SAR data," *IEEE Trans. Geosci. Remote Sens.*, vol. 36, no. 3, pp. 963–973, May 1998.

[27] Y. Yamaguchi, T. Moriyama, M. Ishido, and H. Yamada, "Four-component scattering model for polarimetric SAR image decomposition," *IEEE Trans. Geosci. Remote Sens.*, vol. 43, no. 8, pp. 1699–1706, Aug. 2005.

[28] J. J. van Zyl, M. Arii, and Y. Kim, "Model based decomposition of polarimetric SAR covariance matrices constrained for non-negative eigenvalues," *IEEE Trans. Geosci. Remote Sens.*, vol. 49, no. 9, pp. 3452–3459, Sep. 2011.

[29] M. Arii, J. J. van Zyl, and Y. Kim, "Adaptive model-based decomposition of polarimetric SAR covariance matrices," *IEEE Trans. Geosci. Remote Sens.*, vol. 49, no. 3, pp. 1104–1113, Mar. 2011.

[30] Y. Yamaguchi, A. Sato, W. M. Boerner, R. Sato, and H. Yamada, "Four-component scattering power decomposition with rotation of coherency matrix," *IEEE Trans. Geosci. Remote Sens.*, vol. 49, no. 6, pp. 2251–2258, Jun. 2011.

[31] G. Singh, Y. Yamaguchi, S.-E. Park, Y. Cui, and H. Kobayashi, "Hybrid Freeman/eigenvalue decomposition method with extended volume scattering model," *IEEE Geosci. Remote Sens. Lett.*, vol. 10, no. 1, pp. 81–85, Jan. 2013.

[32] G. Singh, Y. Yamaguchi, and S.-E. Park, "General four-component scattering power decomposition with unitary transformation of coherency matrix," *IEEE Trans. Geosci. Remote Sens.*, vol. 51, no. 5, pp. 3014–3022, May 2013.

[33] S.-W. Chen, X.-S. Wang, S.-P. Xiao, and M. Sato, "General polarimetric model-based decomposition for coherency matrix," *IEEE Trans. Geosci. Remote Sens.*, vol. 52, no. 3, pp. 1843–1855, Mar. 2014.

[34] Y. Cui *et al.*, "On complete model-based decomposition of polarimetric SAR coherency matrix data," *IEEE Trans. Geosci. Remote Sens.*, vol. 52, no. 4, pp. 1991–2001, Apr. 2014.

[35] J.-S. Lee, T. L. Ainsworth, and Y. Wang, "Generalized polarimetric model-based decompositions using incoherent scattering models," *IEEE Trans. Geosci. Remote Sens.*, vol. 52, no. 5, pp. 2474–2491, May 2014.

[36] W. An, Y. Cui, and J. Yang, "Three-component model-based decomposition for polarimetric SAR data," *IEEE Trans. Geosci. Remote Sens.*, vol. 48, no. 6, pp. 2732–2739, Jun. 2010.

[37] G. Franceschetti, A. Iodice, and D. Riccio, "A canonical problem in electromagnetic backscattering from buildings," *IEEE Trans. Geosci. Remote Sens.*, vol. 40, no. 8, pp. 1787–1801, Aug. 2002.

[38] J. S. Lee, D. L. Schuler, and T. L. Ainsworth, "Polarimetric SAR data compensation for terrain azimuth slope variation," *IEEE Trans. Geosci. Remote Sens.*, vol. 38, no. 5, pp. 2153–2163, Sep. 2000.

[39] J. S. Lee *et al.*, "On the estimation of radar polarization orientation shifts induced by terrain slopes," *IEEE Trans. Geosci. Remote Sens.*, vol. 40, no. 1, pp. 30–41, Jan. 2002.
[40] Q. Zhao and R. H. Lang, "Fresnel double scattering from tree branches," *IEEE Trans. Geosci. Remote Sens.*, vol. 50, no. 10, pp. 3640–3647, Oct. 2012.
[41] V. Santalla del Rio, L. Abalde-Lima, and C. G. Christodoulou, "Electromagnetic scattering from vegetation cylindrical components," *IEEE Geosci. Remote Sens. Lett.*, vol. 12, no. 4, pp. 751–755, Apr. 2015.
[42] A. Iodice, A. Natale, and D. Riccio, "Soil moisture retrieval in moderately vegetated areas via a polarimetric two-scale model," in *Proc. IEEE Int. Geosci. Remote Sens. Symp.*, Melbourne, Vic., Australia, Jul. 21–26, 2013, pp. 759–762.
[43] T. J. Jackson and M. H. Cosh, SMEX03 Watershed Ground Soil Moisture Data: Oklahoma, 2006. [Online]. Available: http://nsidc.org/data/amsr_validation/soil_moisture/smex03/index.html
[44] J. F. Moreno, "AGRISAR 2006 agricultural bio-/geophysical retrievals from frequent repeat SAR and optical imaging," European Space Agency, Paris, France, Final Rep., Jan. 2008.
[45] S. Cloude, *Polarisation: Applications in Remote Sensing*. London, U.K.: Oxford Univ. Press, 2009.
[46] J. S. Lee and E. Pottier, *Polarimetric Radar Imaging: From Basics to Applications*. Boca Raton, FL, USA: CRC Press, 2009.
[47] H. Eom and A. Fung, "A scatter model for vegetation up to Ku-band," *Remote Sens. Environ.*, vol. 15, no. 3, pp. 185–200, Jun. 1984.
[48] X. Shen, Q. Qin, Y. Hong, and G. Zhang, "A matrix inversion approach of computing T-matrix for axially symmetrical particles of extreme shape and dielectrically large dimension," *Radio Sci.*, vol. 47, no. 5, Oct. 2012, Art. ID RS5005.
[49] H. T. Hallikainen, F. T. Ulaby, M. C. Dobson, M. A. El-Rayes, and L. K. Wu, "Microwave dielectric behavior of wet soils—Part I: Empirical models and experimental observations," *IEEE Trans. Geosci. Remote Sens.*, vol. GE-23, no. 1, pp. 25–34, Jan. 1985.
[50] G. C. Topp, J. L. Davis, and A. P. Annan, "Electromagnetic determination of soil water content: Measurements in coaxial transmission lines," *Water Resour. Res.*, vol. 16, no. 3, pp. 574–582, Jun. 1980.
[51] V. L. Mironov, L. G. Kosolapova, and S. V. Fomin, "Physically and mineralogically based spectroscopic dielectric model for moist soils," *IEEE Trans. Geosci. Remote Sens.*, vol. 47, no. 7, pp. 2059–2070, Jul. 2009.
[52] E-SAR and F-SAR Leaflets. [Online]. Available: www.dlr.de
[53] ALOS 2 Calibration Results. [Online]. Available: http://www.eorc.jaxa.jp/ALOS-2/en/calval/calval_index.htm
[54] J.-S. Lee, K. W. Hoppel, S. A. Mango, and A. R. Miller, "Intensity and phase statistics of multilook polarimetric and interferometric SAR imagery," *IEEE Trans. Geosci. Remote Sens.*, vol. 32, no. 5, pp. 1017–1028, Sep. 1994.

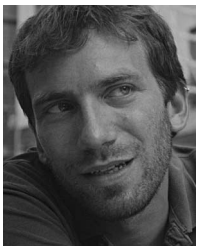

Gerardo Di Martino (S'06–M'09) was born in Naples, Italy, on June 22, 1979. He received the Laurea degree (*cum laude*) in telecommunication engineering and the Ph.D. degree in electronic and telecommunication engineering both from the University of Naples Federico II, Naples, Italy, in 2005 and 2009, respectively.

From 2009 to 2010, he conducted research on indoor electromagnetic propagation and localization of unknown transmitters with the Department of Biomedical, Electronic and Telecommunication Engineering, University of Naples Federico II, through grants from the same university. From 2010 to 2012, he worked on a project financed by the Italian Space Agency aimed at the development of techniques for information extraction from high-resolution SAR images of urban and natural areas. From 2012 to 2014, he was a Research Fellow with the Department of Electrical Engineering and Information Technology, University of Naples Federico II, working on a project regarding maritime surveillance with SAR data. From 2014 to 2015, he conducted research in the field of electromagnetic propagation in harbor scenarios and innovative network architectures through grants received from the Italian National Consortium for Telecommunications. He is currently a Research Fellow with the Department of Electrical Engineering and Information Technology, University of Naples Federico II, working on a project regarding sparse antenna arrays. His main research interests include microwave remote sensing and electromagnetics, with particular focus on modeling of the electromagnetic scattering from natural surfaces and urban areas, SAR signal processing and simulation, information retrieval from SAR data, and remote sensing techniques for developing countries.

Antonio Iodice (S'97–M'00–SM'04) was born in Naples, Italy, in 1968. He received the Laurea degree (*cum laude*) in electronic engineering and the Ph.D. degree in electronic engineering and computer science from the University of Naples Federico II, Naples, Italy, in 1993 and 1999, respectively.

In 1995, he was with the Research Institute for Electromagnetism and Electronic Components, Italian National Council of Research, Naples, and from 1999 to 2000, with Telespazio S.p.A., Rome, Italy. From 2000 to 2004, he was a Research Scientist with the Department of Electronic and Telecommunication Engineering, University of Naples Federico II. He is currently a Professor of electromagnetics with the Department of Electrical Engineering and Information Technology, University of Naples Federico II. He has been involved as a Principal Investigator or Coinvestigator in several projects funded by European Union, Italian Space Agency, Italian Ministry of Education and Research, Campania Regional Government, and private companies. His main research interests include microwave remote sensing and electromagnetism: modeling of electromagnetic scattering from natural surfaces and urban areas, simulation and processing of SAR signals, and electromagnetic propagation in urban areas.

Dr. Iodice serves as the Chair of the IEEE South Italy Geoscience and Remote Sensing Chapter. He received the Sergei A. Schelkunoff Prize Paper Award from the IEEE Antennas and Propagation Society in 2009, for the best paper published in 2008 on the IEEE TRANSACTIONS ON ANTENNAS AND PROPAGATION.

Antonio Natale (M'09) was born in Naples, Italy, on July 3, 1982. He received the B.S. and M.S. degrees (both *cum laude*) in telecommunication engineering and the Ph.D. degree from the University of Naples Federico II, Naples, in 2005, 2008, and 2012, respectively.

In 2011, he was a Visiting Scientist with the Surrey Space Centre, University of Surrey, Surrey, U.K. In that period, he was also the Principal Researcher for the project "Applications for S-band SAR," which was funded by EADS Astrium Ltd. Since April 2012, he has been with the Institute for Electromagnetic Sensing of the Environment, Italian National Research Council, Naples. In 2013, he spent a period at the NATO Centre for Maritime Research and Experimentation, La Spezia, Italy, as a Visiting Scientist to develop target detection and tracking strategies from high-resolution radar data. His research interests include remote sensing, with special regard to the modeling of electromagnetic scattering from natural surfaces, signal processing, and the estimation of parameters from radar data.

Dr. Natale received the 2009 IEEE Geoscience and Remote Sensing South Italy Chapter Prize for the best Italian thesis in remote sensing discussed in 2008. Moreover, he was the recipient of the 2009 S. A. Schelkunoff Transactions Prize Paper Award from the IEEE Antennas and Propagation Society, for the best paper published in 2008 on the IEEE TRANSACTIONS ON ANTENNAS AND PROPAGATION.

Daniele Riccio (M'91–SM'99–F'14) was born in Naples, Italy. He received the Laurea degree (*cum laude*) in electronic engineering from the University of Naples Federico II, Naples, in 1989.

From 1989 to 1994, he was a Research Scientist with the Institute for Research on Electromagnetics and Electronic Components, with the Italian National Research Council. In 1994 and 1995, he was a Guest Scientist with the German Aerospace Centre, Munich, Germany. In 2006, he taught Ph.D. students at the Polytechnic University of Catalonia, Barcelona, Spain, and in 2012, at the Czech Technical University, Prague, Czech Republic. He is currently a Full Professor of electromagnetic theory and remote sensing with the Department of Electrical Engineering and Information Technology, University of Naples Federico II. He is also the Coordinator of the Ph.D. program in information technology and electrical engineering at the same university. He is a member of the Cassini Radar Science Team. He is a Principal Investigator for international research projects on exploitation of remote sensing data and design of SARs and participates in technical committees of international symposia on electromagnetics and remote sensing. His research interests include microwave remote sensing; electromagnetic scattering; SAR with emphasis on sensor design, data simulation and information retrieval; and applications of fractal geometry to remote sensing. He is the author of three books, including *Scattering, Natural Surfaces and Fractals* (2007), and over 350 papers.

Prof. Riccio serves as an Associate Editor for some journals on remote sensing. He received the 2009 Sergei A. Schelkunoff Transactions Prize Paper Award for the best paper published in 2008 on the IEEE TRANSACTIONS ON ANTENNAS AND PROPAGATION.